

5 - JUN 1958

NACA TN 2832

1956

NATIONAL ADVISORY COMMITTEE FOR AERONAUTICS



TECH LIBRARY KAFB, NM

TECHNICAL NOTE 2832

THEORETICAL STUDY OF THE TRANSONIC LIFT OF A DOUBLE-WEDGE PROFILE WITH DETACHED BOW WAVE

By Walter G. Vincenti and Cleo B. Wagoner

Ames Aeronautical Laboratory
Moffett Field, Calif.



Washington

December 1952

AFMCC
TECHNICAL LIBRARY
AFL 2811

U.S.A.F. TECHNICAL LIBRARY
MOLLETT FIELD AIR FORCE BASE
ALAMOGORDO, NEW MEXICO

319 98/39



NATIONAL ADVISORY COMMITTEE FOR AERONAUTICS

TECHNICAL NOTE 2832

THEORETICAL STUDY OF THE TRANSONIC LIFT OF A DOUBLE-WEDGE

PROFILE WITH DETACHED BOW WAVE¹

By Walter G. Vincenti and Cleo B. Wagoner.

SUMMARY

A theoretical study is described of the aerodynamic characteristics at small angle of attack of a thin, double-wedge profile in the range of supersonic flight speed in which the bow wave is detached. The analysis is carried out within the framework of the transonic (nonlinear) small-disturbance theory, and the effects of angle of attack are regarded as a small perturbation on the flow previously calculated at zero angle. The mixed flow about the front half of the profile is calculated by relaxation solution of a suitably defined boundary-value problem for the transonic small-disturbance equation in the hodograph plane (i.e., the Tricomi equation). The purely supersonic flow about the rear half is found by an extension of the usual numerical method of characteristics.² Analytical results are also obtained, within the framework of the same theory, for the range of speed in which the bow wave is attached and the flow is completely supersonic.

The calculations provide, for vanishingly small angle of attack, the following information as a function of the transonic similarity parameter: (1) chordwise lift distribution, (2) lift-curve slope, and (3) position of center of lift. As in previous studies, the aerodynamic characteristics of a profile of given thickness ratio show little variation with free-stream Mach number as the Mach number passes through 1. As the Mach number is increased to higher values, however, the lift-curve slope rises to a pronounced maximum in the vicinity of shock attachment and then declines. Correspondingly, the center of lift moves forward toward the leading edge and then returns aft. These findings are in marked contrast to the behavior of the drag coefficient at zero angle of attack, which was found in earlier work to decrease monotonically as the Mach number increased above 1. At Mach numbers above that for shock attachment, the results of the present calculations tend toward those given by classical linear theory.

¹Portions of this work were reported at the VIIIth International Congress on Theoretical and Applied Mechanics, Istanbul, Turkey, August 20-28, 1952.

INTRODUCTION

The theoretical problem of the transonic flow over a thin, double-wedge profile at zero angle of attack has been treated in several papers in recent years. These papers have in common that they employ the simplifying concepts of the transonic small-disturbance theory and utilize the hodograph transformation to linearize the resulting mathematical problem. Following this approach, Guderley and Yoshihara (reference 1) began by solving the problem for a free-stream Mach number of 1, using analytical methods for the mixed flow over the front wedge and the method of characteristics for the purely supersonic flow over the rear. Somewhat later, the present authors, using a combination of relaxation methods and the method of characteristics (references 2 and 3), extended the results to free-stream Mach numbers greater than 1, where a detached bow wave occurs ahead of the profile. At about the same time, Cole (reference 4) obtained an analytical solution for the flow over the front wedge at subsonic flight speeds, utilizing, in effect, the special assumption of a vertical sonic line from the shoulder of the wedge. More recently, Trilling (reference 5) has been able to remove this special assumption and, with the aid of less stringent approximations regarding the flow over the rear wedge, to extend the solution for the subsonic case to include the complete profile. As a result of these investigations, the problem of the double-wedge profile at zero angle of attack may be regarded as substantially solved within the limitations of the transonic small-disturbance theory. The experimental studies of Liepmann and Bryson (references 6 and 7) and Griffith (reference 8) indicate that the theoretical findings are in fundamental agreement with the physical facts.

In a recent paper (reference 9), Guderley and Yoshihara have continued their investigations of the double-wedge profile at Mach number 1 by considering the influence of a vanishingly small angle of attack. The basic idea in this later work is to regard the effects of angle of attack as a first-order perturbation on the nonlinear flow previously calculated at zero angle. This approach leads to a linear boundary-value problem in both the physical and hodograph planes. The calculation for the front wedge is still carried out, however, in the hodograph plane, since the basic procedures can then be taken over directly from the previous work. By this means, Guderley and Yoshihara obtain results for the lift-curve slope of the profile at zero angle of attack and for the corresponding distribution of lift along the chord.

The aim of the present paper is to extend the results for the double wedge at angle of attack to the case of supersonic flight with detached bow wave. The fundamental ideas of Guderley and Yoshihara are followed in reducing the calculations for the front wedge to a perturbation problem in the hodograph plane. The detailed formulation of the problem is, however, necessarily different in the present case. The

boundary conditions for the problem appear in terms of the results already obtained at zero lift (references 2 and 3), and the solution is carried out by numerical methods which differ only slightly from those devised for the earlier work. The lift on the rear wedge is calculated by an extension of the method of characteristics. The body of the paper is devoted to the detailed formulation of the boundary-value problem in the hodograph plane and to a discussion of the final results. Noteworthy differences between the numerical procedures used in the present work and those already described in reference 3 are treated in appendices at the end of the report.

NOTATION

Primary Symbols

a_*	critical speed (i.e., speed at which the speed of flow and the speed of sound are equal)
b	numerical coefficient (See equations (39) and (40).)
c	airfoil chord
c_l	lift coefficient $\left(\frac{\text{lift per unit span}}{q_0 c} \right)$
c_m	moment coefficient for moments taken about leading edge $\left(\frac{\text{moment per unit span}}{q_0 c^2} \right)$
C_p	pressure coefficient $\left(\frac{p - p_0}{q_0} \right)$
I_w	integral defined by equation (45)
k_2	numerical constant (See equation (10).)
M	Mach number
m	slope of segment of Mach line in characteristics net
p	static pressure

Δp	local lifting pressure (i.e., difference between static pressures on upper and lower surfaces)
q	dynamic pressure
t	airfoil thickness
V	speed of flow
x, y	Cartesian coordinates
X, Y	generalized Cartesian coordinates (See equations (43).)
$\left(\frac{x}{c}\right)_l$	chordwise position of center of lift
$\left(\frac{dc_l}{d\alpha}\right)_{\alpha=0}$	slope of curve of lift coefficient versus true angle of attack evaluated at zero angle
$\left(\frac{dc_m}{d\alpha}\right)_{\alpha=0}$	slope of curve of moment coefficient versus true angle of attack evaluated at zero angle
α	normalized angle of attack; also denotes true angle of attack when used in derivatives such as $\frac{dc_l}{d\alpha}$, etc.
β	absolute value of η at left-hand limit of lattice
γ	ratio of specific heats (1.4 for air)
Δ	basic lattice interval
ξ	function of η and θ (See equation (A6).)
$\eta, \tilde{\eta}$	normalized speed of flow (See equation (1a) and page 10.)
η_1, η_2	special values of η (See sketch (m) on page 46.)
$\theta, \tilde{\theta}$	normalized inclination of flow; θ also denotes true inclination of flow in equation (lb) (See equation (lb) and page 10.)
θ_w	normalized half angle of wedge
ξ_0	transonic similarity parameter (See equation (13).)

ρ fluid density

ψ stream function

$\delta\psi_A$ incremental values of stream function
(See equations (A9) and (A11).)

Subscripts

a,b,c points in characteristics net
(See page 43.)

A,B components of total stream function
(See equation (39).)

o conditions in free stream

s singular solution
(See equations (A6) and (A7).)

o,1,2,
etc. value at a prescribed lattice point

* conditions at critical speed

Superscripts

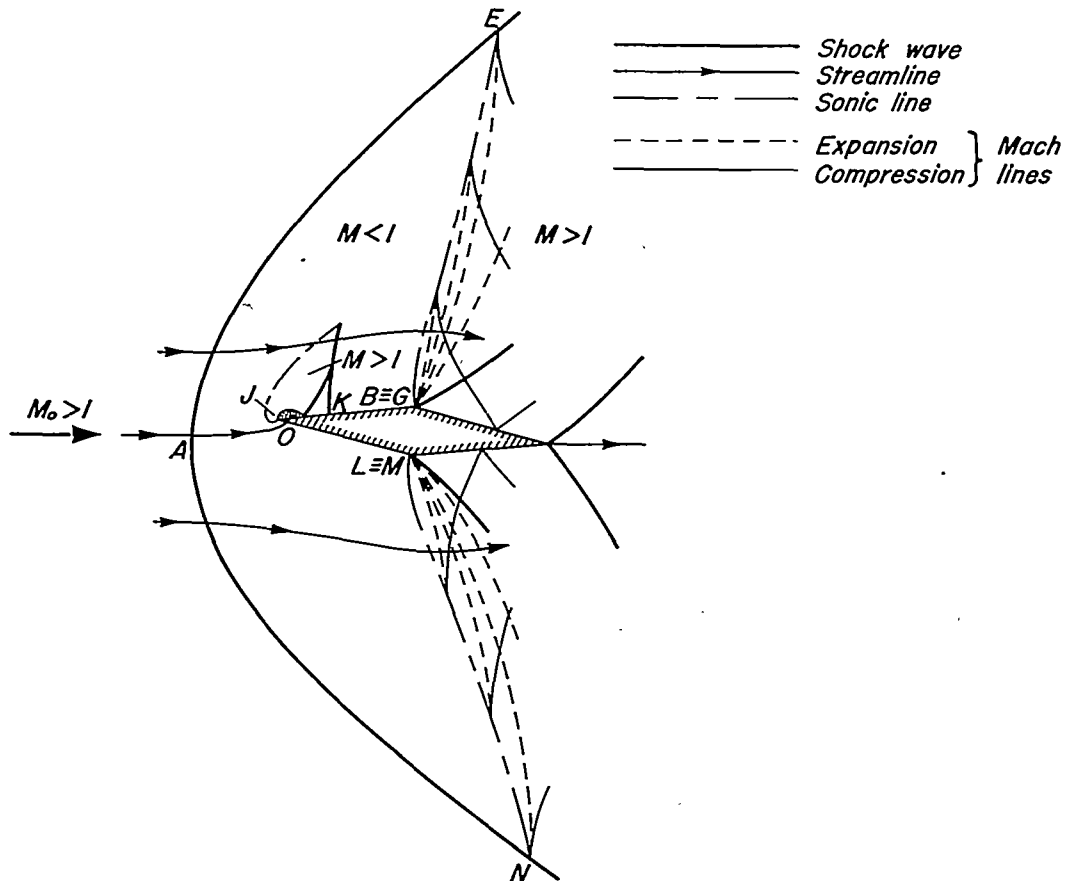
($\bar{}$) quantities determined at zero angle of attack

($\dot{\ } \cdot$) derivative with respect to normalized angle of attack
evaluated at zero angle

BOUNDARY-VALUE PROBLEM IN HODOGRAPH PLANE

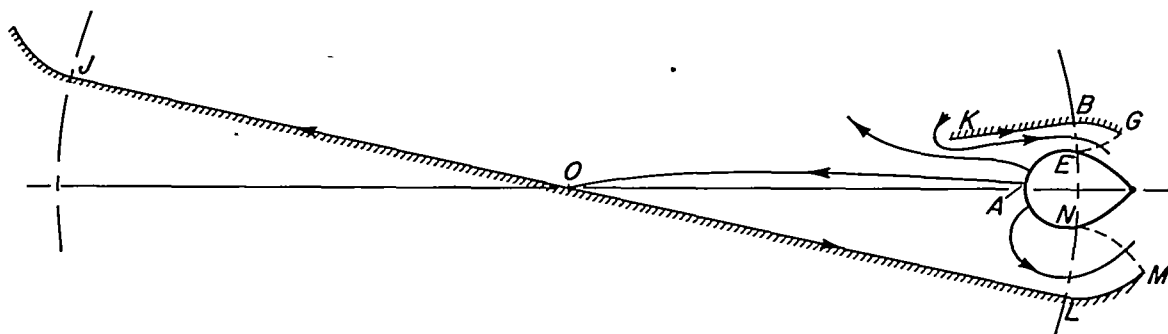
Description of Flow Field

Sketch (a) is a drawing of the idealized, inviscid flow which



Sketch (a)

may be expected about a wedge profile when the angle of attack is sufficiently less than the semiapex angle of the wedge. Sketch (b)



Sketch (b)

shows the corresponding hodograph representation of the flow over the front wedge, which is the region of prime theoretical concern. Except for the substitution of the detached bow wave in place of the infinite free stream, these representations follow the lines assumed by Guderley and Yoshihara in reference 9. The corresponding drawings for zero angle of attack, which are fundamental to the present case, have been described in detail in references 2 and 3.

In the present example, the path of the central streamline in the physical and hodograph planes is briefly as follows: The streamline leaves the bow wave in the physical plane (or the shock polar in the hodograph plane) at point A. It then proceeds with decreasing subsonic speed to a stagnation point O on the underside of the profile. At O the streamline branches. The lower branch runs downstream along the lower surface of the profile with fixed inclination but increasing speed. The sonic speed is reached at the shoulder L, where the speed then increases discontinuously in accord with the Prandtl-Meyer relations. The shoulder itself maps in the hodograph onto the upgoing characteristic LM. The upper branch of the central streamline proceeds from O upstream along the surface of the profile. The inclination here is again fixed by that of the surface, and the speed increases to the sonic value at the leading edge J. At this point the flow is characterized by another Prandtl-Meyer expansion to supersonic speed.

The flow configuration which should be assumed on the upper surface near the leading edge is open to conjecture. Since the geometrically available angle of turn will, for any thin airfoil, be greater than the 130° permissible for expansion to a vacuum, a region of separation is to be expected. If the angle of attack is not too great, this region will probably be closed, with the central streamline reattaching to the upper surface a small distance behind the leading edge. This reattachment will be followed by a compression of the flow through a system of shock waves whose arrangement is sketched only formally in the physical plane (and not at all in the hodograph plane, where the correct representation would probably lie on several sheets). The effects of the flow near the leading edge will be mentioned later, but the exact process will remain undefined. Whatever the details, the speed on the upper surface will return to a subsonic value at some point K just downstream of a terminating, normal shock wave. From K the central streamline continues at fixed inclination downstream along the upper surface, the speed increasing once more to the sonic value at the shoulder B. At this point another expansion takes place, similar to that which occurs at the corresponding point on the lower surface. In this case the shoulder is represented in the hodograph by the down-going characteristic BG.

The supersonic expansion fan from the shoulder at B (and similarly at L) is discussed in detail in references 2 and 3. Suffice it here to say that the supersonic flow field, of which the expansion fan is the

initial part, is separated into two regions by the Mach line GE, which runs from the shoulder to the sonic point on the bow wave. (This line was termed the "separating" Mach line in reference 2.) The supersonic flow in the region upstream of the Mach line GE is interdependent with the subsonic field between the bow wave and sonic line. To obtain a solution for the front wedge, a problem in transonic flow must therefore be solved for the subsonic field and the interdependent portion of the supersonic expansion fan. Conditions in the supersonic flow downstream of the Mach line GE have no influence upon the subsonic field. The continuation of the flow beyond GE can be accomplished by purely supersonic methods once the solution of the transonic problem is known.

Aside from the obvious lack of symmetry in the present case, the main difference between the flow here and that previously studied at zero angle of attack is the existence in the present problem of the localized supersonic region in the vicinity of the nose. As pointed out, conditions in this region are difficult to formulate. The problem has been considered by Guderley and Yoshihara (reference 9) in the course of their work at Mach number 1. They find that, if the nose region is disregarded in the hodograph and the boundary condition along KB is fulfilled all the way in to 0, then the influence on the lift of the resulting fictitious flow at the nose is of somewhat higher than the second order in the angle of attack. This suggests that the effects of the real flow at the nose may be neglected in a first-order analysis such as the present. In the work which follows, as in the calculations of Guderley and Yoshihara, the supersonic region at the leading edge will therefore be disregarded.

Formulation of Boundary-Value Problem

As in reference 3, the analysis is based on the equations of the transonic small-disturbance theory with the stream function ψ as the dependent variable. If the effects of the flow at the nose are ignored, the problem of the wedge at angle of attack α is then readily formulated as a boundary-value problem in the hodograph plane. To solve this problem for vanishingly small α , it will be assumed that the solution ψ at angle of attack can be expressed as the sum of the basic solution $\tilde{\psi}$ previously obtained at zero angle plus a perturbation term $\alpha\psi'$, where ψ' is a function which does not itself involve α . By consideration of the difference between the boundary-value problems for ψ and $\tilde{\psi}$, a problem for the perturbation function ψ' can be formulated. The boundaries for this problem turn out to be the same as those for the problem at zero angle, and the boundary values themselves appear in terms of $\tilde{\psi}$. The details of these matters will now be given. The reader who is interested only in the results can turn directly to the section Chordwise Distribution of Lift on page 28.

Basic equations. - The basic equations will be taken in the form given in reference 3, that is, in terms of small disturbances from the critical speed a_* .² The independent variables are the normalized speed $\tilde{\eta}$ and the normalized inclination $\tilde{\theta}$ as defined by the relations

$$\tilde{\eta} = \frac{V/a_* - 1}{V_o/a_* - 1} \quad (1a)$$

$$\tilde{\theta} = \left(\frac{2}{\gamma+1} \right)^{1/2} \frac{\theta}{(V_o/a_* - 1)^{3/2}} \quad (1b)$$

where

V local speed of flow

θ local inclination of flow relative to direction of free stream

V_o free-stream speed

a_* critical speed (i.e., speed at which the speed of flow and the speed of sound are equal)

γ ratio of specific heats

Use of these variables is equivalent to introducing the rules for transonic similarity. In terms of the foregoing hodograph variables, the differential equation for the stream function ψ as given by the transonic small-disturbance theory is

$$\psi_{\tilde{\eta}\tilde{\eta}} - 2\tilde{\eta} \psi_{\tilde{\theta}\tilde{\theta}} = 0 \quad (2)$$

²As discussed in several recent papers (e.g., references 10 and 11), the theory can also be formulated in terms of disturbances from the free-stream speed V_o . This latter, less restrictive formulation reveals clearly the relationship which exists between the transonic small-disturbance theory and the familiar linear theory of subsonic or supersonic flow. As shown by Spreiter (see page 9 of reference 11), an a_* analysis will yield values of the pressure coefficient identical to those of a V_o analysis provided the pressure coefficient and similarity parameter in the former case are taken as in equations (4) and (13) below. If this procedure is followed, the results of the a_* analysis may even be expected to tend toward those of linear theory as the free-stream Mach number increases or decreases from 1. (An analytical example of just this behavior has been given by Bryson in appendix A of reference 7.) It appears, therefore, that the a_* formulation, when suitably used, gives results of wider theoretical validity than would be anticipated on the basis of its own rather restrictive underlying assumption.

This is essentially the linear differential equation first studied by Tricomi (reference 12). It is elliptic for $\tilde{\eta} < 0$ (subsonic speeds) and hyperbolic for $\tilde{\eta} > 0$ (supersonic speeds).

The transformation from the hodograph to the physical plane is governed by the differential relations

$$\frac{dx}{d\tilde{\eta}} = \frac{1}{\rho_* a_*} \left[\frac{(\gamma+1)(V_0/a_* - 1)}{2} \right]^{1/2} (2\tilde{\eta}\psi_\theta d\tilde{\eta} + \psi_{\tilde{\eta}} d\tilde{\theta}) \quad (3a)$$

$$\frac{dy}{d\tilde{\eta}} = \frac{1}{\rho_* a_*} (\psi_{\tilde{\eta}} d\tilde{\eta} + \psi_{\tilde{\theta}} d\tilde{\theta}) = \frac{1}{\rho_* a_*} d\psi \quad (3b)$$

where $x=x(\tilde{\eta}, \tilde{\theta})$ and $y=y(\tilde{\eta}, \tilde{\theta})$ are physical coordinates (horizontal and vertical, respectively) corresponding to a given velocity $\tilde{\eta}, \tilde{\theta}$. The symbol ρ_* denotes the fluid density at the critical speed a_* . Within the approximation of the transonic small-disturbance theory, the pressure coefficient $C_p \equiv (p-p_0)/q_0$ can be calculated from the relation

$$C_p = -2 \frac{V-V_0}{a_*} = -2(V_0/a_* - 1)(\tilde{\eta} - 1) \quad (4)$$

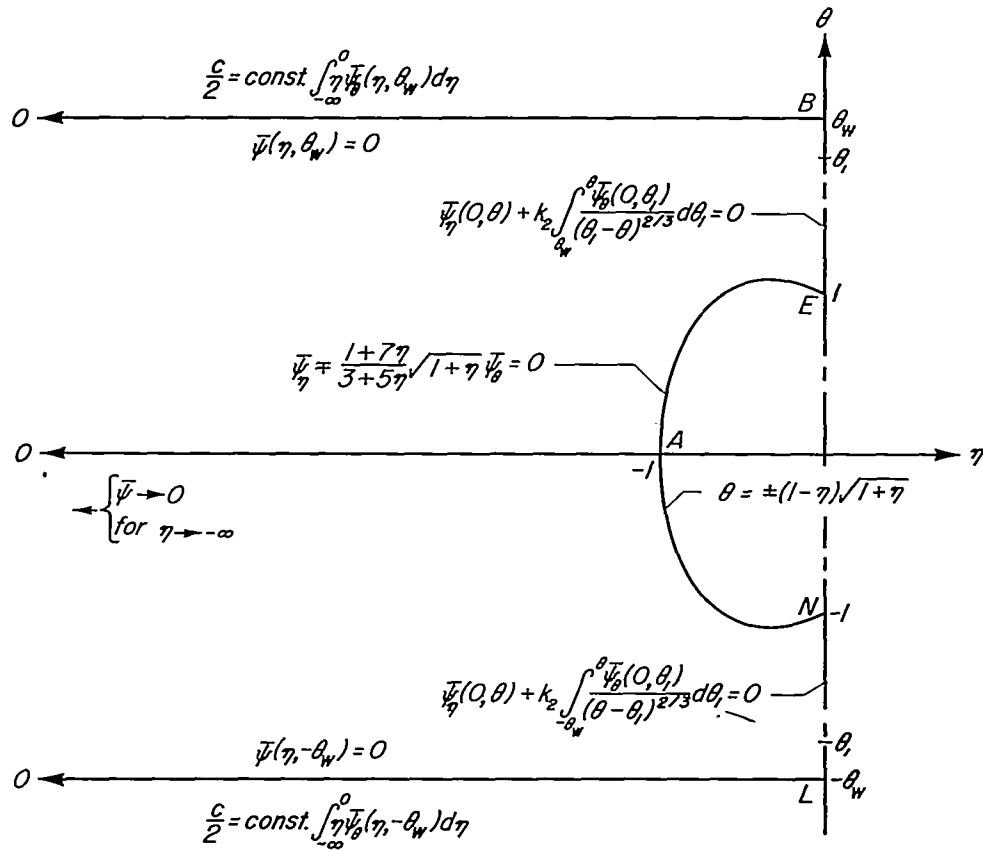
The local Mach number is related to the speed of flow by the equation

$$\frac{M^2 - 1}{\gamma + 1} = \frac{V}{a_*} - 1 \quad (5)$$

For simplicity of notation, the tilde will be omitted from the symbols $\tilde{\eta}$ and $\tilde{\theta}$ in the remainder of the development. It is to be understood, unless stated otherwise, that the quantities η and θ are themselves the normalized quantities defined by equations (1).

Problem at zero angle of attack. - When the angle of attack is zero, the localized region of supersonic flow at the leading edge disappears from sketch (a), and the flow field becomes symmetrical about the chord line. The corresponding boundary-value problem in the η, θ plane has

been set forth in reference 3. It is restated in sketch (c), where both the upper and lower halves of the flow field are now included. In this representation, the surfaces of the wedge appear as the semi-infinite horizontal lines OB and OL, and the subsonic portion of the shock polar appears as the curve NAE.



Sketch (c)

If the stream function for zero angle of attack is denoted by $\bar{\psi} = \bar{\psi}(\eta, \theta)$, the differential equation to be satisfied here is given by equation (2) as

$$\bar{\psi}_{\eta\eta} - 2\eta \bar{\psi}_{\theta\theta} = 0 \quad (6)$$

The requirement that the flow shall be tangent to the surfaces of the wedge provides the boundary conditions

$$\bar{\psi}(\eta, \pm\theta_w) = 0 \quad \text{for } \eta \leq 0 \quad (7)$$

where θ_w denotes the normalized half-angle at the leading edge. The stagnation point at the leading edge is represented in the present theory by the condition that

$$\bar{\psi} \rightarrow 0 \quad \text{for } \eta \rightarrow -\infty, \quad -\theta_w \leq \theta \leq \theta_w \quad (8)$$

Along the shock polar NAE, the relations for an oblique shock wave require that

$$\bar{\psi}_\eta + \frac{1+7\eta}{3+5\eta} \sqrt{1+\eta} \bar{\psi}_\theta = 0 \quad (9)$$

for

$$\theta = \pm (1-\eta) \sqrt{1+\eta}, \quad -1 \leq \eta \leq 0$$

Along the sonic line, boundary conditions are prescribed which represent the influence exerted on the subsonic field by the interdependent portion of the supersonic expansion fans. On the basis of the procedures given in reference 3, this influence can be represented completely by the requirement that

$$\bar{\psi}_\eta(0, \theta) + k_2 \int_{\pm\theta_w}^0 \frac{\bar{\psi}_\theta(0, \theta_1)}{[\pm(\theta_1 - \theta)]^{2/3}} d\theta_1 = 0 \quad (10)$$

where the upper signs apply for $1 \leq \theta \leq \theta_w$ and the lower signs for $-\theta_w \leq \theta \leq -1$. The constant k_2 which appears here is given by

$$k_2 = \frac{2^{4/3} \pi}{3^{1/6} \Gamma^3(1/3)} \approx 0.3429$$

where $\Gamma(1/3)$ is the gamma function of the argument $1/3$. The use of the relations (10) as boundary conditions along the sonic line reduces the transonic problem of the flow over the front wedge to a purely elliptic problem in the hodograph plane.

In addition to the foregoing conditions, a further condition is necessary to assure that the solution for ψ will give the proper scale when transformed to the physical plane. This is furnished, for example, by the following expression for the half-chord of the profile, found by integrating equation (3a) over either OB or OL:

$$\frac{c}{2} = \frac{2}{\rho_* a_*} \left[\frac{(\gamma+1)(V_0/a_* - 1)}{2} \right]^{1/2} \int_{-\infty}^0 \eta \bar{\psi}_\theta(\eta, \pm \theta_w) d\eta \quad (11)$$

If the chord of the profile is given, this condition, together with the previous conditions (7) through (10), is sufficient to determine a unique solution to the problem.

It is obvious from the nature of the boundary-value problem (and also from considerations of symmetry in the physical plane) that the solution for ψ must be antisymmetric with respect to θ . The problem can be simplified, therefore, by discarding the lower half of the hodograph and replacing it by the condition

$$\bar{\psi}(\eta, 0) = 0 \quad \text{for } \eta \leq -1 \quad (12)$$

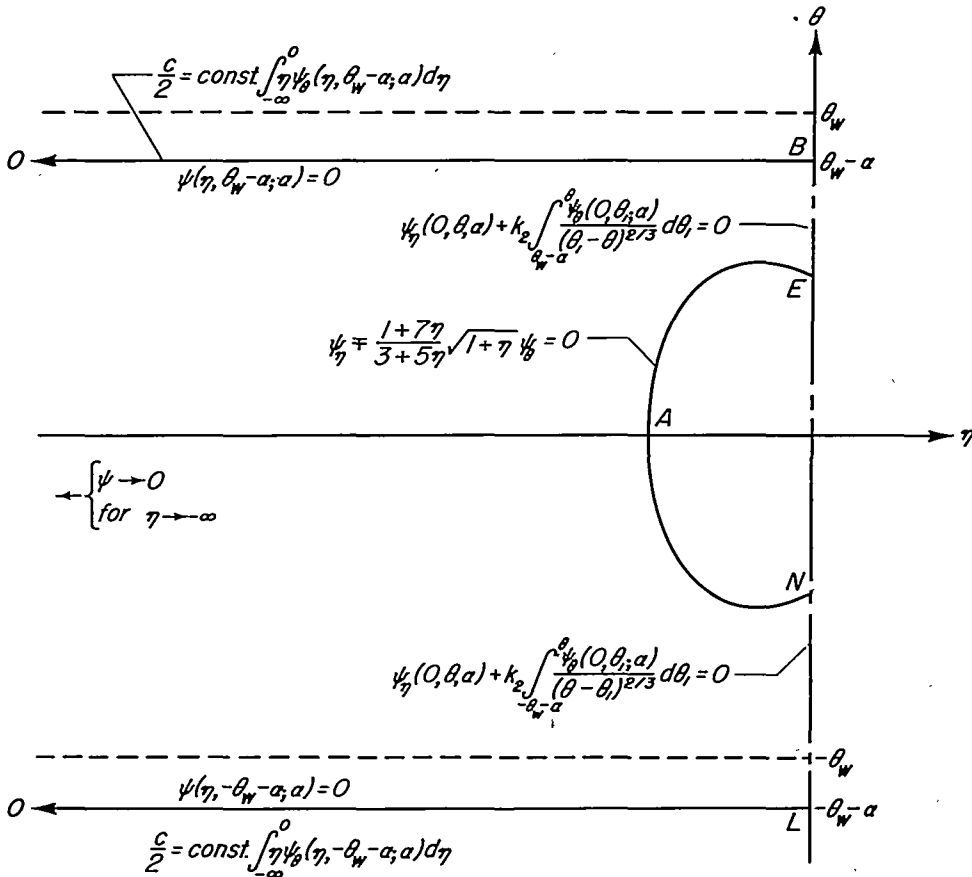
The resulting problem is readily solved with numerical methods by assuming an arbitrary value of $\bar{\psi}$ at some point (as, for example, point E), solving for $\bar{\psi}$ in the upper half of the hodograph subject to the conditions (7), (8), (9), (10), and (12), and then adjusting the solution to satisfy condition (11).

It is apparent from the boundary conditions that the solution of the foregoing problem will depend on the value of the parameter θ_w , which defines the position of the upper and lower boundaries in the hodograph. This parameter is related to the more familiar transonic similarity parameter ξ_0 by the relation

$$\xi_0 \equiv \frac{M_0^2 - 1}{[(\gamma+1)(t/c)]^{2/3}} = \frac{2^{1/3}}{\theta_w^{2/3}} \quad (13)$$

where t/c is the thickness ratio of the complete double-wedge profile. In references 2 and 3 the solution of the foregoing problem has been carried out for four values of θ_w .

Problem at angle of attack. - If the supersonic region at the leading edge is ignored, the boundary-value problem for the wedge at angle of attack appears in the η, θ plane as shown in sketch (d).



Sketch (d)

The primary difference between this and the previous sketch is that the lines OB and OL, which represent the surfaces of the wedge, have each been displaced downward by an amount α , where α is the angle of attack normalized in the same manner as the other angles of inclination (cf. equation (1b)).³

³In reference 9, Guderley and Yoshihara find it convenient to obtain the angle of attack by holding the profile fixed and changing the inclination of the free stream. This procedure, if applied in the present case, would require the eventual calculation of the second derivatives of ψ on the shock polar. The present procedure, which holds the free stream fixed and changes the attitude of the profile, requires the calculation of only a first derivative of ψ at the surface of the wedge. Since the accuracy of numerical differentiation decreases with increasing order of the derivative, the present approach is to be preferred in a numerical analysis.

The stream function at angle of attack will be denoted here by $\psi = \psi(\eta, \theta; \alpha)$, the latter notation being used to indicate the dependence of ψ upon the parameter α . The function ψ must satisfy the differential equation (2), which is now written

$$\psi_{\eta\eta} - 2\eta\psi_{\theta\theta} = 0 \quad (14)$$

The boundary conditions at the surface of the wedge now require that

$$\psi(\eta, \pm\theta_w - \alpha; \alpha) = 0 \quad \text{for } \eta \leq 0 \quad (15)$$

while the condition at the leading edge becomes

$$\psi \rightarrow 0 \quad \text{for } \eta \rightarrow -\infty, \quad -\theta_w - \alpha \leq \theta \leq \theta_w - \alpha \quad (16)$$

The shock polar NAE is unaltered from the previous problem, and the condition on this boundary has the same form as before. The conditions along the segments BE and LN of the sonic line are now

$$\psi_\eta(0, \theta; \alpha) + k_2 \int_{\pm\theta_w - \alpha}^{\theta} \frac{\psi_\theta(0, \theta_1; \alpha)}{[\pm(\theta_1 - \theta)]^{2/3}} d\theta_1 = 0 \quad (17)$$

where the lower limit of the integral has been changed in accord with the displacement of the points B and L. The upper signs in equation (17) now apply for $1 \leq \theta \leq \theta_w - \alpha$ and the lower signs for $-\theta_w - \alpha \leq \theta \leq -1$. An expression for the half-chord of the profile can be found again by integrating equation (3a) over the line OB or OL, which gives

$$\frac{c}{2} = \frac{2}{\rho_* \alpha_*} \left[\frac{(\gamma+1)(V_0/a_* - 1)}{2} \right]^{1/2} \int_{-\infty}^0 \eta \psi_\theta(\eta, \pm\theta_w - \alpha; \alpha) d\eta \quad (18)$$

If the chord of the airfoil is specified - say the same as at zero angle of attack - then the foregoing conditions are sufficient to determine a solution. No simplification based on symmetry considerations is possible in the present case.

Perturbation problem. - The problem of the preceding section conceivably could be solved by numerical methods - though with great labor - for arbitrary values of α . Efforts in this direction would hardly be justified, however, in view of the fundamental omission of the localized supersonic flow at the leading edge. It is more reasonable to examine the problem for vanishingly small α , where this omission is valid and where there is hope that the amount of labor might be reduced.

To proceed along these lines, it is assumed that $\psi(\eta, \theta; \alpha)$ may be expanded in a power series of the form

$$\psi(\eta, \theta; \alpha) = \psi(\eta, \theta; 0) + \alpha \psi_\alpha(\eta, \theta; 0) + O(\alpha^2)$$

where, for present purposes, only terms to order α need be retained. The first term on the right represents the solution at $\alpha = 0$ and is thus identical with the function $\bar{\psi}(\eta, \theta)$ previously introduced. The second term will be abbreviated by means of the notation $\psi'(\eta, \theta) \equiv \psi_\alpha(\eta, \theta; 0)$. If terms of $O(\alpha^2)$ are discarded, the expression for ψ can then be written

$$\psi(\eta, \theta; \alpha) = \bar{\psi}(\eta, \theta) + \alpha \psi'(\eta, \theta) \quad (19)$$

By comparison of the previous boundary-value problems for ψ and $\bar{\psi}$, a problem for the perturbation function ψ' will now be formulated.

The differential equation for ψ' follows at once from the differential equations (6) and (14) and the substitution (19). It is obviously of the same form as the previous equations, that is,

$$\psi'_{\eta\eta} - 2\eta \psi'_{\theta\theta} = 0 \quad (20)$$

The boundary conditions appropriate to the surface of the wedge are established as follows: The boundary condition (15) for ψ is first rewritten, with the aid of the substitution (19), in the form

$$\bar{\psi}(\eta, \pm\theta_w - \alpha) + \alpha \psi'(\eta, \pm\theta_w - \alpha) = 0 \quad (21)$$

By expanding in Taylor's series about the lines $\theta = \pm\theta_w$, the functions $\bar{\psi}$ and ψ' can be written

$$\bar{\psi}(\eta, \pm\theta_w - \alpha) = \bar{\psi}(\eta, \pm\theta_w) - \alpha \bar{\psi}_\theta(\eta, \pm\theta_w) + O(\alpha^2) \quad (22a)$$

$$\psi'(\eta, \pm\theta_w - \alpha) = \psi'(\eta, \pm\theta_w) - \alpha \psi'_\theta(\eta, \pm\theta_w) + O(\alpha^2) \quad (22b)$$

If these expansions are substituted into equation (21) and $\bar{\psi}(\eta, \pm\theta_w)$ set equal to zero in accord with the boundary condition (7), one obtains finally for vanishingly small α

$$\psi'(\eta, \pm\theta_w) = \bar{\psi}_\theta(\eta, \pm\theta_w) \quad \text{for } \eta \leq 0 \quad (23)$$

This is the boundary condition for ψ' appropriate to the surface of the profile. It will be noted that the condition is applied in the hodograph at the original, undeflected location of the surface (i.e., $\theta = \pm \theta_w$). The condition depends for its application on a knowledge of the basic solution Ψ .

The boundary condition for ψ' at the leading edge follows directly from the conditions (8) and (16). It is the same as the corresponding condition for $\bar{\Psi}$, that is,

$$\psi' \rightarrow 0 \quad \text{for } \eta \rightarrow -\infty, \quad -\theta_w \leq \theta \leq \theta_w \quad (24)$$

As was indicated, the functions ψ and $\bar{\Psi}$ both satisfy the same linear, homogeneous boundary condition on the shock polar. It follows, as in the case of the differential equation, that the condition for ψ' on the polar is again the same, that is,

$$\psi'_\eta + \frac{1+7\eta}{3+5\eta} \sqrt{1+\eta} \psi'_\theta = 0 \quad (25)$$

for

$$\theta = \pm(1-\eta)\sqrt{1+\eta}, \quad -1 \leq \eta \leq 0$$

The treatment of the boundary condition along the sonic line is complicated by the fact that the parameter α appears in the condition (17) as a term in the lower limit of the integral. For simplicity, the details will be confined here to the upper segment BE of the sonic line. For this segment, condition (17) becomes, after substitution from equation (19),

$$\bar{\Psi}_\eta(0, \theta) + \alpha \psi'_\eta(0, \theta) + k_2 \int_{\theta_w-\alpha}^{\theta} \frac{\bar{\Psi}_\theta(0, \theta_1)}{(\theta_1-\theta)^{2/3}} d\theta_1 + \alpha k_2 \int_{\theta_w-\alpha}^{\theta} \frac{\psi'_\theta(0, \theta_1)}{(\theta_1-\theta)^{2/3}} d\theta_1 = 0 \quad (26)$$

applicable for $1 \leq \theta \leq \theta_w - \alpha$. To simplify this equation, the first integral is rewritten

$$\int_{\theta_w-\alpha}^{\theta} \frac{\bar{\Psi}_\theta(0, \theta_1)}{(\theta_1-\theta)^{2/3}} d\theta_1 = \int_{\theta_w}^{\theta} \frac{\bar{\Psi}_\theta(0, \theta_1)}{(\theta_1-\theta)^{2/3}} d\theta_1 - \int_{\theta_w}^{\theta_w-\alpha} \frac{\bar{\Psi}_\theta(0, \theta_1)}{(\theta_1-\theta)^{2/3}} d\theta_1 \quad (27)$$

It can be shown from Guderley's analysis of flow at a convex corner (reference 13) that, for vanishingly small values of $(\theta_w - \theta)$, the variation of $\bar{\psi}$ along the sonic line must be of the form

$$\bar{\psi}(0, \theta) = \bar{C} (\theta_w - \theta)^{4/3} \quad (28)$$

where \bar{C} is a constant for any given value of θ_w . Differentiating this relation, one obtains

$$\bar{\psi}_\theta(0, \theta_1) \sim (\theta_w - \theta_1)^{1/3}$$

Substitution of this result into the second integral of equation (27) yields the fact that this integral must be proportional to $\alpha^{4/3}$. The first integral in equation (26) can thus be written

$$\int_{\theta_w-\alpha}^{\theta} \frac{\bar{\psi}_\theta(0, \theta_1)}{(\theta_1 - \theta)^{2/3}} d\theta_1 = \int_{\theta_w}^{\theta} \frac{\bar{\psi}_\theta(0, \theta_1)}{(\theta_1 - \theta)^{2/3}} d\theta_1 + O(\alpha^{4/3}) \quad (29)$$

The second integral of equation (26) can be treated similarly by first rewriting it as

$$\int_{\theta_w-\alpha}^{\theta} \frac{\psi'_\theta(0, \theta_1)}{(\theta_1 - \theta)^{2/3}} d\theta_1 = \int_{\theta_w}^{\theta} \frac{\psi'_\theta(0, \theta_1)}{(\theta_1 - \theta)^{2/3}} d\theta_1 - \int_{\theta_w}^{\theta_w-\alpha} \frac{\psi'_\theta(0, \theta_1)}{(\theta_1 - \theta)^{2/3}} d\theta_1 \quad (30)$$

To deduce the variation of ψ' for vanishingly small $(\theta_w - \theta)$, it is first noted that a result similar to equation (28) must also hold for the variation of ψ relative to the displaced location of the shoulder, that is,

$$\psi(0, \theta) = C (\theta_w - \alpha - \theta)^{4/3}$$

The quantity $C = C(\alpha)$ is a differentiable function of α which reduces to \bar{C} when $\alpha = 0$. Since α will eventually be made less than any assignable value of $(\theta_w - \theta)$, this expression may be expanded in the form

$$\psi(0, \theta) = C (\theta_w - \theta)^{4/3} \left[1 - \frac{4}{3} \frac{\alpha}{\theta_w - \theta} + O(\alpha^2) \right] \quad (31)$$

Now it follows from the definition of ψ' that

$$\psi'(0, \theta) = \lim_{\alpha \rightarrow 0} \frac{\psi(0, \theta) - \bar{\psi}(0, \theta)}{\alpha}$$

Substitution from equations (28) and (31) thus gives for the variation of ψ' in the vicinity of the shoulder

$$\psi'(0, \theta) = \lim_{\alpha \rightarrow 0} \left[\frac{C - \bar{C}}{\alpha} (\theta_w - \theta)^{4/3} - \frac{4}{3} C (\theta_w - \theta)^{1/3} + O(\alpha) \right]$$

or

$$\psi'(0, \theta) = C' (\theta_w - \theta)^{4/3} - \frac{4}{3} C (\theta_w - \theta)^{1/3} \quad (32)$$

where $C' \equiv C_\alpha(0)$. This means that for vanishingly small $(\theta_w - \theta)$

$$\psi'_\theta(0, \theta_1) \sim (\theta_w - \theta_1)^{-2/3}$$

On the basis of this result equation (30) can be written

$$\int_{\theta_w - \alpha}^{\theta} \frac{\psi'_\theta(0, \theta_1)}{(\theta_1 - \theta)^{2/3}} d\theta_1 = \int_{\theta_w}^{\theta} \frac{\psi'_\theta(0, \theta_1)}{(\theta_1 - \theta)^{2/3}} d\theta_1 + O(\alpha^{1/3}) \quad (33)$$

If equations (29) and (33) are substituted into equation (26) and the boundary condition (10) is taken into account, one then obtains for vanishingly small α

$$\psi'_\eta(0, \theta) + k_2 \int_{\theta_w}^{\theta} \frac{\psi'_\theta(0, \theta_1)}{(\theta_1 - \theta)^{2/3}} d\theta_1 = 0 \quad (34)$$

where $1 \leq \theta \leq \theta_w$. The boundary condition for ψ' along the upper segment of the sonic line is thus the same as the condition for $\bar{\psi}$. The same result can be shown to hold along the lower segment.

It remains to impose the condition that the chord of the airfoil must remain unaltered during change in angle of attack. To express this condition in terms of ψ' , equation (19) is first substituted into equation (18) to obtain

$$\frac{c}{2} = \frac{2}{\rho_* a_*} \left[\frac{(\gamma+1)(V_0/a_* - 1)}{2} \right]^{1/2} \int_{-\infty}^0 \eta \left[\bar{\psi}_\theta(\eta, \pm \theta_w - \alpha) + \alpha \psi'_\theta(\eta, \pm \theta_w - \alpha) \right] d\eta \quad (35)$$

As in the treatment of the boundary conditions along the upper and lower boundaries, Taylor's expansion gives

$$\bar{\Psi}_\theta(\eta, \pm\theta_w - \alpha) = \bar{\Psi}_\theta(\eta, \pm\theta_w) - \alpha \bar{\Psi}_{\theta\theta}(\eta, \pm\theta_w) + O(\alpha^2) \quad (36a)$$

$$\psi'_\theta(\eta, \pm\theta_w - \alpha) = \psi'_\theta(\eta, \pm\theta_w) - \alpha \psi'_{\theta\theta}(\eta, \pm\theta_w) + O(\alpha^2) \quad (36b)$$

It can be inferred directly from the boundary-value problem for $\bar{\Psi}$ that $\bar{\Psi}_{\theta\theta}(\eta, \pm\theta_w) = 0$, so that the term involving this quantity may be dropped from equation (36a). Substitution of equations (36) into equation (35) and application of the previous expression (11) leads, for vanishingly small α , to the condition that

$$\int_{-\infty}^0 \eta \psi'_\theta(\eta, \pm\theta_w) d\eta = 0 \quad (37)$$

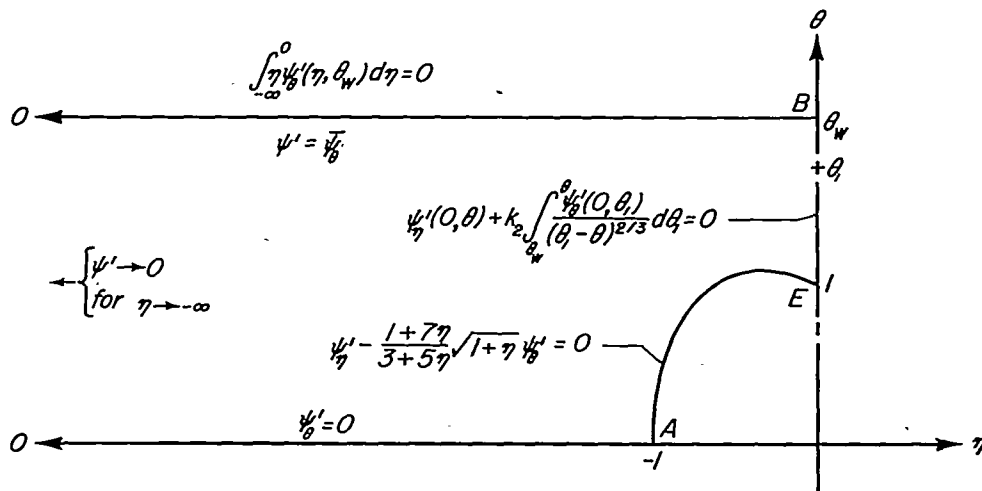
The boundary conditions (23), (24), (25), (34), and (37) are sufficient to determine the solution for ψ' in the hodograph.

As with $\bar{\Psi}$, the boundary-value problem for ψ' can be simplified from considerations of symmetry. Since $\bar{\Psi}$ is antisymmetric with respect to θ , the nonhomogeneous boundary condition (23) which is imposed on ψ' along the upper and lower boundaries must be symmetric in this variable. The remaining conditions, which are all homogeneous, are also symmetric. It follows that ψ' itself must be a symmetric function of θ .⁴ The problem can therefore be simplified by again eliminating the lower half of the hodograph and substituting in this case the condition that

$$\psi'_\theta(\eta, 0) = 0 \quad \text{for } \eta \leq -1 \quad (38)$$

⁴This result can also be argued directly from considerations in the physical plane. It is necessary to make two observations as follows: (1) Since the profile itself is symmetric about the chord line, the flow field at a negative angle of attack must be the inverted image of the flow field at an equal positive angle. (2) To be consistent with the basic perturbation assumption, it must be presumed that all changes in the flow field are smooth functions of angle of attack at $\alpha = 0$. These statements taken together imply that the vertical distance between any two points of equal η and corresponding positive and negative θ is, to a first order, unaffected by angle of attack. It follows that, for sufficiently small α , the increments in ψ and $\bar{\Psi}$ between the two points are equal and hence, on the basis of equation (19), that the value of ψ' at the two points is the same.

The problem which is finally to be solved is thus as summarized in sketch (e). The boundaries for this problem are identical with those used to obtain $\bar{\Psi}$. The boundary conditions are also identical insofar as the shock polar and sonic line are concerned. The only differences between the two problems are in the conditions imposed along the boundaries OB and OA. As was the case with $\bar{\Psi}$, the solution here must be a function of θ_w .

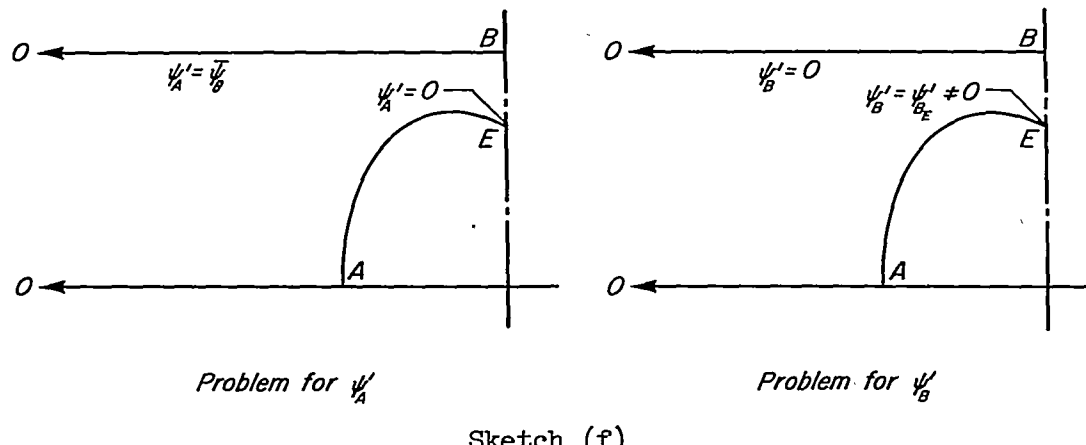


Sketch (e)

Because of the nature of the integral condition along the upper boundary OB, a direct solution for ψ' is not feasible by numerical methods. To obtain a solution, therefore, the problem is broken down into two subsidiary problems by means of the substitution

$$\psi' = \psi'_A + b\psi'_B \quad (39)$$

where b is a constant whose value is to be determined. Boundary-value problems for ψ'_A and ψ'_B are then defined as shown in sketch (f).



Sketch (f)

In both problems the integral condition along the upper boundary OB is ignored for the time being, and an arbitrary condition is introduced instead at the point E. In the problem for ψ'_A , only the nonhomogeneous condition (23) is imposed at the upper boundary, and the condition at E is the homogeneous one that $\psi'_A = 0$. In the problem for ψ'_B , the homogeneous condition $\psi'_B = 0$ is imposed along OB, and the condition at E is that ψ'_B has an arbitrary value $\psi'_{BE} \neq 0$. The conditions at the remaining boundaries are the same as in sketch (e) and are therefore not repeated here. It is apparent that a superposition of ψ'_A and ψ'_B will constitute a solution of the original problem provided the value of b is adjusted so that the integral condition (37) is satisfied on the upper boundary. The necessary equation for b is found by substituting the expression (39) into condition (37) and is

$$b = - \frac{\int_{-\infty}^0 \eta \psi'_{A\theta}(\eta, \theta_w) d\eta}{\int_{-\infty}^0 \eta \psi'_{B\theta}(\eta, \theta_w) d\eta} \quad (40)$$

Relations for quantities in physical plane. - To complete the fundamental analysis, relations must be established between ψ' and the relevant quantities in the physical plane. Let $\bar{x} = \bar{x}(\eta, \theta)$ and $\bar{y} = \bar{y}(\eta, \theta)$ denote the coordinates at which a given velocity η, θ is found in the physical plane when the profile is at zero angle of attack. As shown in reference 3 (pp. 29-31), the transformation equations (3), when applied to the case of zero angle of attack (and written in the present notation), can be put in the dimensionless form

$$d\left(\frac{\bar{x}}{c}\right) = \frac{1}{4\bar{I}_w} (2\eta\bar{\psi}_\theta d\eta + \bar{\psi}_\eta d\theta) \quad (41a)$$

$$[(\gamma+1)(t/c)]^{1/3} d\left(\frac{\bar{y}}{c}\right) = \frac{(2\theta_w)^{1/3}}{4\bar{I}_w} (\bar{\psi}_\eta d\eta + \bar{\psi}_\theta d\theta) = \frac{(2\theta_w)^{1/3}}{4\bar{I}_w} d\bar{\psi} \quad (41b)$$

where \bar{I}_w represents the integral

$$\bar{I}_w = \int_{-\infty}^0 \eta \bar{\psi}_\theta(\eta, \theta_w) d\eta \quad (42)$$

By taking the origin of the physical coordinates at the leading edge and introducing the notation $\bar{X} = \bar{x}/c$ and $\bar{Y} = [(\gamma+1)(t/c)]^{1/3}(\bar{y}/c)$, equations (41) can be integrated to give

$$\bar{Z}(\eta, \theta) = \frac{1}{4\bar{I}_W} \int_C (2\eta\bar{\psi}_\theta d\eta + \bar{\psi}_\eta d\theta) \quad (43a)$$

$$\bar{Y}(\eta, \theta) = \frac{(2\theta_W)^{1/3}}{4\bar{I}_W} \bar{\psi} \quad (43b)$$

The integration in equation (43a) is performed in the hodograph over any curve C which begins at $\eta = -\infty$ and ends at the point η, θ . The generalized coordinates X and Y at which the same velocity η, θ is to be found when the airfoil is at angle of attack are given correspondingly by

$$X(\eta, \theta; \alpha) = \frac{1}{4I_W} \int_C (2\eta\psi_\theta d\eta + \psi_\eta d\theta) \quad (44a)$$

$$Y(\eta, \theta; \alpha) = \frac{(2\theta_W)^{1/3}}{4I_W} \psi \quad (44b)$$

The integration in equation (44a) is considered to be taken over the same curve C as before.⁵ The integral I_W is now given by

$$I_W \equiv \int_{-\infty}^0 \eta\psi_\theta(\eta, \theta_W - \alpha) d\eta \quad (45)$$

It can be shown from equations (19), (36), and (37) that for vanishingly small α

$$I_W = \bar{I}_W \quad (46)$$

Equations (44) can now be specialized in the light of the basic perturbation assumption. This assumption implies at once that the coordinates X and Y in the physical plane must be expressible in the form

⁵If C lies slightly outside the domain in which ψ is defined - as will be the case, for example, when the integration is taken over the upper surface of the wedge in its undisplaced position - ψ is to be thought of as being continued analytically outside the boundary.

$$X(\eta, \theta; \alpha) = \bar{X}(\eta, \theta) + \alpha X'(\eta, \theta) \quad (47a)$$

$$Y(\eta, \theta; \alpha) = \bar{Y}(\eta, \theta) + \alpha Y'(\eta, \theta) \quad (47b)$$

where $X'(\eta, \theta) \equiv X_\alpha(\eta, \theta; 0)$ and $Y'(\eta, \theta) \equiv Y_\alpha(\eta, \theta; 0)$. If expressions (19) and (47) are substituted into equations (44), and equations (43) and (46) are taken into account, the following relations are finally obtained for X' and Y' in terms of ψ' :

$$X'(\eta, \theta) = \frac{1}{4\bar{I}_W} \int_C (2\eta\psi'_\theta d\eta + \psi'_\eta d\theta) \quad (48a)$$

$$Y'(\eta, \theta) = \frac{(2\theta_W)^{1/3}}{4\bar{I}_W} \psi' \quad (48b)$$

The foregoing equations (48) give the initial rate of movement with angle of attack of a point of fixed velocity η, θ . One requires for practical application, however, the rate of change of η and θ at a point of fixed location X, Y . Equations relating the two sets of derivatives can be obtained as follows: If η and θ are regarded in the physical plane as functions of X, Y , and α - that is, $\eta = \eta(X, Y; \alpha)$ and $\theta = \theta(X, Y; \alpha)$ - then the corresponding total differentials are

$$d\eta = \eta_X dX + \eta_Y dY + \eta_\alpha d\alpha \quad (49a)$$

$$d\theta = \theta_X dX + \theta_Y dY + \theta_\alpha d\alpha \quad (49b)$$

Consistent with the basic perturbation assumption, η and θ can be written

$$\eta(X, Y, \alpha) = \bar{\eta}(\bar{X}, \bar{Y}) + \alpha \eta'(\bar{X}, \bar{Y}) \quad (50a)$$

$$\theta(X, Y, \alpha) = \bar{\theta}(\bar{X}, \bar{Y}) + \alpha \theta'(\bar{X}, \bar{Y}) \quad (50b)$$

where $\bar{\eta}$ and $\bar{\theta}$ represent the conditions at a given point \bar{X}, \bar{Y} at zero angle of attack and η' and θ' are defined by $\eta'(\bar{X}, \bar{Y}) \equiv \eta_\alpha(\bar{X}, \bar{Y}; 0)$, $\theta'(\bar{X}, \bar{Y}) \equiv \theta_\alpha(\bar{X}, \bar{Y}; 0)$. In view of equations (50), equations (49) can be written for vanishingly small α

$$d\eta = \bar{\eta}_X dX + \bar{\eta}_Y dY + \eta' d\alpha \quad (51a)$$

$$d\theta = \bar{\theta}_X dX + \bar{\theta}_Y dY + \theta' d\alpha \quad (51b)$$

Similarly, from equations (47), one can write for the differentials of X and Y as functions of η , θ , and α

$$dX = \bar{X}_\eta d\eta + \bar{X}_\theta d\theta + X' d\alpha$$

$$dY = \bar{Y}_\eta d\eta + \bar{Y}_\theta d\theta + Y' d\alpha$$

from which

$$\bar{X}_\eta d\eta + \bar{X}_\theta d\theta = dX - X' d\alpha \quad (52a)$$

$$\bar{Y}_\eta d\eta + \bar{Y}_\theta d\theta = dY - Y' d\alpha \quad (52b)$$

Solution of equations (52) for $d\eta$ and $d\theta$ and comparison of the results with the alternative expressions (51) gives finally for η' and θ'

$$\eta' = - \frac{\bar{Y}_\theta X' - \bar{X}_\theta Y'}{\bar{X}_\eta \bar{Y}_\theta - \bar{X}_\theta \bar{Y}_\eta} \quad (53a)$$

$$\theta' = \frac{\bar{Y}_\eta X' - \bar{X}_\eta Y'}{\bar{X}_\eta \bar{Y}_\theta - \bar{X}_\theta \bar{Y}_\eta} \quad (53b)$$

These equations can be put in more directly useful form by evaluating the derivatives of \bar{X} and \bar{Y} from equations (43) and substituting for X' and Y' from equations (48). There results finally

$$\eta'(\bar{X}, \bar{Y}) = - \frac{1}{2\eta\bar{\psi}_\theta^2 - \bar{\psi}_\eta^2} \left[\bar{\psi}_\theta \int_C (2\eta\psi'_\theta d\eta + \psi'_\eta d\theta) - \bar{\psi}_\eta \psi' \right] \quad (54a)$$

$$\theta'(\bar{X}, \bar{Y}) = \frac{1}{2\eta\bar{\psi}_\theta^2 - \bar{\psi}_\eta^2} \left[\bar{\psi}_\eta \int_C (2\eta\psi'_\theta d\eta + \psi'_\eta d\theta) - 2\eta\bar{\psi}_\theta \psi' \right] \quad (54b)$$

By means of these equations the initial rate of change of η and θ at some fixed point in the physical plane can be calculated corresponding to any chosen location in the hodograph. The coordinates at which these derivatives apply are found from the solution at zero angle of attack by means of equations (43).

The foregoing equations are considerably simplified when applied at the surface of a wedge profile. Here the boundary condition is that $\bar{\Psi}$ is constant on a line of constant θ (cf. equation (7)), with the result that $\bar{\Psi}_\eta = 0$. Equation (54a), for example, can thus be written as simply

$$\eta'(\bar{X}, \pm 0) = - \frac{1}{\bar{\eta} \bar{\Psi}_\theta(\eta, \pm \theta_w)} \int_{-\infty}^{\bar{\eta}} \eta \psi'_\theta(\eta, \pm \theta_w) d\eta \quad (55)$$

where the upper signs pertain to the upper surface and the lower signs to the lower surface. The corresponding rate of change of pressure coefficient is found by differentiating equation (4) with respect to angle of attack. If α is used now to denote the true angle of attack (related to the previously used, normalized angle of attack by an equation like (1b)), such differentiation then gives

$$\left(\frac{dC_p}{d\alpha} \right)_{\alpha=0} = -2 \left(\frac{2}{\gamma+1} \right)^{1/2} \frac{1}{(V_0/a_* - 1)^{1/2}} \eta'$$

Here η' is still the derivative with respect to the normalized angle as given by equations (54a) or (55). With the aid of equations (5) and (13), this result can be rewritten

$$[(\gamma+1)(t/c)]^{1/3} \left(\frac{dC_p}{d\alpha} \right)_{\alpha=0} = -2(2\theta_w)^{1/3} \eta' \quad (56)$$

It can be seen from equation (55) and the symmetry properties of $\bar{\Psi}$ and ψ' that η' must be of equal magnitude but opposite sign on the upper and lower surfaces of the profile. If the local lift coefficient is represented by $\Delta p/q_0 \equiv (p_{\text{lower}} - p_{\text{upper}})/q_0$, it then follows from equation (56) that

$$[(\gamma+1)(t/c)]^{1/3} \left[\frac{d(\Delta p/q_0)}{d\alpha} \right]_{\alpha=0} = 4(2\theta_w)^{1/3} \eta'(\bar{X}, +0) \quad (57)$$

where the notation $\eta'(\bar{X}, +0)$ indicates that the value is to be taken on the upper surface of the profile. Substitution from equation (55) gives finally

$$[(\gamma+1)(t/c)]^{1/3} \left[\frac{d(\Delta p/q_0)}{d\alpha} \right]_{\alpha=0} = - \frac{4(2\theta_w)^{1/3}}{\bar{\eta} \bar{\Psi}_\theta(\bar{\eta}, \theta_w)} \int_{-\infty}^{\bar{\eta}} \eta \psi'_\theta(\eta, \theta_w) d\eta \quad (58)$$

By means of this equation, the initial rate of growth of lift at any chordwise station can be obtained. Since $\bar{\Psi}$ and ψ' are both functions

of the parameter θ_w , the generalized quantity which appears on the left-hand side of equation (57) is also a function of this parameter. These results are in conformity with the rules for transonic similarity (see, for example, reference 11).

METHOD OF SOLUTION

As in the previous calculations of $\bar{\psi}$, the boundary-value problems for ψ'_A and ψ'_B can be solved through the use of finite-difference equations and relaxation techniques. A detailed description of the general method has been given in reference 3 and need not be repeated here. Most of the necessary finite-difference equations - notably the tedious ones along the shock polar and sonic line - can be taken over directly from the previous work. The only equations which need be altered are those directly influenced by the change in boundary conditions on the upper boundary and on the horizontal axis. The only real difficulty from this source is encountered in the solution for ψ'_A in the vicinity of the shoulder (point B in sketch (f)). At the shoulder itself, the boundary conditions require a singularity in the first derivatives of ψ'_A , which means that any purely numerical treatment would be of doubtful validity in the vicinity of this point. This difficulty is overcome by subtracting out an analytical solution of the proper singular form and then working locally with the difference between this solution and the desired unknown. The singular solution is obtained from the general results of Guderley (reference 13) and is expressed in terms of hypergeometric functions. The details of this and other matters regarding the numerical calculations for the front half of the profile are given in appendix A.

With the solution known for the front half of the profile, the calculation of the lift on the rear half is a simple matter. The computations are carried out in the physical plane and are based on the characteristics net previously constructed for the flow over the rear wedge at zero angle of attack (see, for example, fig. 4 of reference 3). Starting from the known solution for ψ' , one first employs equations (48) to compute the initial rate of movement of the points at which the Mach lines of the basic characteristics net meet the sonic line. Using these results and the known slope of the segments of the basic net, one then proceeds stepwise along consecutive downgoing Mach lines, calculating the initial rate of movement of successive intersection points on each line. By application of the proper boundary conditions at the surface of the wedge, the value of η' at the surface is finally determined, and from this the initial distribution of lift is calculated. The details of the procedure are given in appendix B.

RESULTS AND DISCUSSION

Calculations of the lift have been carried out, following the methods just outlined, for the same values of θ_w used in the work at zero lift, namely, 1.3, 1.6, 2.4, and 4.2. These values correspond, respectively (see equation (13)), to values of the similarity parameter ξ_0 of 1.058, 0.921, 0.703, and 0.484.

To illustrate the results for the front wedge in the hodograph, figures 1 to 3 have been prepared showing the variation of ψ'_A , ψ'_B , and ψ' for $\theta_w = 1.6$.⁶ The results for ψ'_B (fig. 1) are only slightly different from those previously shown for ψ in figure 3 of reference 3. As before, a rapid (but regular) variation is apparent in the dependent variable in the vicinity of the point $\eta = 0$, $\theta = 1$. The results for ψ'_A (fig. 2) show a rapid variation near the point $\eta = 0$, $\theta = \theta_w$. This is a consequence of the previously mentioned singularity in the first derivatives of ψ'_A at that point. The values of ψ' (fig. 3) are found in the present case from the equation $\psi' = \psi'_A - 0.5348 \psi'_B$ (cf. equation (39)). They exhibit the same behavior as does ψ'_A in the vicinity of the singular point but differ markedly in other parts of the field. For reference, the numerical values from which figures 1 and 2 were plotted are given in tabular form at the end of the report.

The complete results for the lift of the profile are given in figures 4 through 7. These results will be discussed in the following paragraphs.

Chordwise Distribution of Lift

Figure 4 is a plot of the calculated lift distribution, in transonic similarity form, for the four values of ξ_0 considered in the present work. Also shown are the results for $\xi_0 = 0$ ($M_\infty = 1$) given by Guderley and Yoshihara in reference 9. It is convenient for purposes of discussion to think of a similarity plot, such as that of figure 4, as pertaining to fixed values of t/c and γ . From this standpoint, an increase from zero in the similarity parameter ξ_0 is equivalent to an increase from 1 in the free-stream Mach number M_∞ . For simplicity, this point of view will sometimes be adopted in the descriptions that follow.

⁶For the calculation of ψ'_B in this example, use was made of 236 lattice points distributed as shown for ψ in figure 2 of reference 3. For ψ'_A , 380 points were used with a distribution appropriate to the altered behavior of the dependent variable.

The lift distributions of figure 4 are all of the same general shape. In all cases the calculated lift tends toward infinity at the leading edge of the profile. This type of result, which is of course physically impossible, is well known from the linear theory of airfoils at subsonic speeds. It is a result of the obvious failure of the small-disturbance approximations to conform with the actual phenomena in the vicinity of the leading edge. This local failure of the theory is known in the linear, subsonic case to be of little consequence insofar as the over-all lift is concerned. It may be presumed that a similar situation exists here.

As one proceeds rearward from the leading edge, the lift distribution falls more or less rapidly, reaching a value of zero directly forward of the shoulder. This latter result could have been foreseen, since the speed on both the upper and lower surfaces has a fixed (i.e., sonic) value at this location. Directly to the rear of the shoulder, the lift distribution starts anew from zero. This must obviously be the case, since the expansion from sonic speed is, in Prandtl-Meyer flow, a unique function of the local turning angle, which is the same for both surfaces. Rearward from the shoulder the lift increases monotonically to a relatively small, finite value at the trailing edge.

Over the front wedge, the four curves of the present study exhibit a uniform progression with respect to ξ_0 . The curve of Guderley and Yoshihara, however, crosses the present curves at several points. The reasons for this are not clear, though it is highly unlikely that such a result could be in fact correct. The observed behavior may be due to some consistent inaccuracy in the present numerical approach or to the approximations introduced by Guderley and Yoshihara in satisfying the boundary conditions for the interdependent portion of the supersonic expansion fan. Over the rear wedge, the present computations give virtually a single curve for the four values of ξ_0 . There is again, however, a small inconsistency with the results given by Guderley and Yoshihara. This is as might be expected if the calculated flow over the front wedge is in error in either case.

Lift-Curve Slope

Figure 5 shows the generalized slope of the lift curve at zero angle of attack plotted as a function of the transonic similarity parameter. Results obtained on the basis of the transonic small-disturbance theory are shown by three solid-line curves. Each of these curves consists of two segments separated by a gap within which the curve cannot be defined on the basis of the available results. The uppermost of the three curves gives the lift of the complete profile; the other two show the division of lift between the front and rear wedges.

The left-hand segment of each of the curves in figure 5 shows the variation of lift-curve slope over most of the range of flight speed in which the bow wave is detached, which is the range of primary concern in the present analysis. The calculated points from which these curves were drawn are shown in the figure. The points denoted by squares were obtained by mechanical integration of the lift-distribution curves of figure 4.⁷ The circled points on the vertical axis were located on the basis of the work of Guderley and Yoshihara.

The right-hand segment of the curves in figure 5 shows the variation of lift-curve slope in the range of flight speed in which the bow wave is attached and the flow is completely supersonic. To the order of accuracy of the present theory, this condition exists for the double-wedge profile at zero angle of attack when $\xi_0 \geq 2^{1/3} = 1.260$.⁸ Above this value, results completely consistent with the fundamental assumptions of the transonic small-disturbance theory can easily be obtained by analytical methods. To this end, one need only presume that the speed is constant on each straight-line portion of the airfoil surface, a condition which is actually fulfilled over most of the pertinent range of ξ_0 . The necessary procedures are outlined in appendix C. To the accuracy of the transonic small-disturbance theory, the results provide an exact solution for the lift-curve slope of the front wedge for all values of ξ_0 in the range of completely supersonic flow. For the rear wedge - and hence for the complete profile - the solution is exact down to a limiting value of ξ_0 somewhat greater than 1.260. Below this limit the interaction of the shock wave from the bow and the expansion fan from the shoulder influences the flow over the rear wedge, with the result that the condition of constant speed is not satisfied. The position of this limit is difficult to determine exactly. As shown in appendix C, however, it must lie at a value of ξ_0 less than 1.287. The curves for the rear wedge and complete profile are thus approximate for at least a portion of the interval from 1.287 to 1.260 and are therefore shown dotted in this range. It can be demonstrated that inclusion of the interaction effects in the analysis would cause an increase in the computed lift for the rear wedge. Exact results would thus lie somewhere above the dotted portion of the curves in figure 5.

⁷As in the earlier calculations of the drag coefficient at zero angle (cf. page 36 of reference 3), the integration over a small interval near the leading edge was carried out analytically on the basis of an asymptotic representation of the solution in the hodograph plane.

⁸Attachment of the wave takes place at the somewhat lower value of $\xi_0 = 3/(4)^{2/3} = 1.191$. For $1.191 < \xi_0 < 1.260$ the wave is attached but the flow behind it is still subsonic.

The most interesting aspect of figure 5 is the behavior of the lift in the vicinity of shock attachment. Despite the gap in the curves in this vicinity, it is obvious that the lift-curve slope of the complete profile must attain a maximum somewhere in the range from $\xi_0 = 1.058$ to $\xi_0 = 1.287$. This is in marked - and somewhat surprising - contrast to the previous results for the drag coefficient at zero angle of attack, which was found (reference 2) to decrease monotonically as the similarity parameter increased above zero. The peak in the curve in the present case is accompanied by a similar variation in the lift-curve slope of the front wedge. The results for the rear wedge may or may not pass through a minimum in the same range of ξ_0 .

A determination of the exact shape of the curves in the vicinity of shock attachment is not feasible on the basis of the present laborious methods. The existing curve for the complete profile does show a maximum in the range of completely supersonic flow, but this is in the portion of the range in which the computed curve is known to be erroneously low. If exact results were available for all values of ξ_0 , the maximum would undoubtedly be somewhat higher and displaced somewhat to the left. The infinity which appears in the slope of the curve at $\xi_0 = 1.260$ (see appendix C) would probably disappear as well. The lift of the rear wedge, which now goes to zero at $\xi_0 = 1.260$, would presumably remain finite throughout.

Within the transonic range itself, the curves of figure 5 show little variation for some distance above a similarity parameter of zero. This is in accord with Guderley's recent analytical study of two-dimensional flows with a free-stream Mach number close to 1 (reference 14). The results of Guderley's work imply that, to the accuracy of the small-disturbance theory, the lift-curve slope does not vary as the free-stream Mach number passes through 1. The curves of figure 5 have been faired so as to conform with this requirement. It is apparent that Guderley's result of zero variation may be taken as a good working approximation even at Mach numbers some distance removed from 1. The same result was found in reference 3 with regard to the drag coefficient of the complete profile at zero angle of attack.

Over most of the range of completely supersonic flow, the lift-curve slope of the complete profile exhibits the type of variation well known from linear theory. This latter theory gives for the lift-curve slope of all thin profiles

$$\frac{dc_l}{d\alpha} = \frac{4}{(M_\infty^2 - 1)^{1/2}} \quad (59)$$

which can be written in terms of the transonic similarity variables as

$$[(\gamma+1)(t/c)]^{1/3} \frac{dc_l}{d\alpha} = \frac{4}{\xi_0^{1/2}} \quad (60)$$

The dashed curve in figure 5 is based on this equation. There is considerable quantitative difference between the linear and nonlinear results for values of ξ_0 just above 1.287. As ξ_0 increases, however, the curves given by the two theories appear to converge. This latter behavior is in accord with Spreiter's considerations (reference 11) regarding the basic relationship between the linear and nonlinear theories.

To put the results in more familiar form, the lift-curve slope of the complete profile has been replotted in figure 6 as a function of Mach number for $\gamma = 1.4$. The results of linear theory give a unique curve defined by equation (59). The nonlinear, transonic theory provides a family of curves with thickness ratio as a parameter.⁹ As would be expected, the range of Mach numbers over which the linear theory is a poor approximation becomes smaller as the thickness ratio is reduced. It can be reasoned, in fact, that the nonlinear results must tend toward the results of the linear theory as $t/c \rightarrow 0$.

Center of Lift

Figure 7 shows the chordwise position of the center of lift (x/c)_l as a function of the transonic similarity parameter. The arrangement of the figure parallels that of figure 5. As before, the indicated points were calculated on the basis of the lift distributions of figure 4. The curve in the range of completely supersonic flow ($\xi_0 \geq 1.260$) was obtained by means of the equations of appendix C. Only results for the complete profile are shown.

⁹Here, as in reference 2, a multiplicity of curves could be obtained for each thickness ratio by using expressions for the pressure coefficient and similarity parameter different from those of equations (4) and (13). In view of the recent developments outlined in footnote 2, such complications now appear to be of lessened significance.

The movement of the center of lift with increasing Mach number is of some interest. At a free-stream Mach number of 1, the results of Guderley and Yoshihara indicate a position about 29 percent of the chord aft of the leading edge. As the Mach number is increased, the center of lift first moves forward, slowly in the initial stages and then more rapidly as the condition for shock attachment is approached. In the completely supersonic range, this trend is reversed; the center of lift then moves aft toward the midchord location given by linear theory. Apparently, the reversal of the direction of motion must take place rather suddenly in the vicinity of shock attachment. The limit of forward movement cannot be specified, except to say that it must lie somewhere ahead of 22 percent of the chord (and probably aft of the leading edge). The dotted (i.e., inexact) portion of the curve passes precisely through the quarter-chord point at $\xi_0 = 1.260$. (The corresponding lift distribution is one of uniform lift on the front wedge and zero lift on the rear.) Because of the interaction effects previously discussed, an exact result would lie somewhat above the dotted curve.

CONCLUDING REMARKS

The present calculations add support to the growing conclusion (see references 2, 6, 7, 8, and 14) that no marked changes take place in characteristics of airfoil sections as the free-stream Mach number passes through 1. The establishment of this conclusion must be regarded, in fact, as one of the major successes of recent research in transonic flow. In the present case, as in the previous study of the drag coefficient at zero lift, the variation of the aerodynamic quantities with free-stream Mach number is most rapid in the vicinity of shock attachment. Unlike the behavior of the drag coefficient, however, the variations here are large and characterized by a sudden reversal in the sign of the derivative. In drawing conclusions from these results it must be remembered, of course, that the theory assumes an inviscid medium and an airfoil of small thickness and infinite span. It also assumes, in effect, that the angle of attack is of an order smaller than the thickness ratio. To what extent the results will be valid for viscous flows about finite-span airfoils at practically usable values of the thickness ratio and angle of attack is difficult to say. The effects of

finite span, for example, will surely cause a reduction in the variations near shock attachment. In the present state of theoretical development, the study of these effects is a task for experiment.

Ames Aeronautical Laboratory
National Advisory Committee for Aeronautics
Moffett Field, Calif., Aug. 1, 1952

APPENDIX A
SOLUTION OF BOUNDARY-VALUE PROBLEM
FOR FRONT WEDGE IN HODOGRAPH PLANE

The solution of the boundary-value problems for ψ'_A and ψ'_B was accomplished by finite-difference methods similar to those developed for the calculation of $\bar{\psi}$ in reference 3. The description here will be limited to the few features wherein the present work departs from that discussed in the earlier paper. (See general remarks under METHOD OF SOLUTION.) The notation and sketches follow the conventions used in reference 3.

Finite-Difference Equations Common to Both Problems

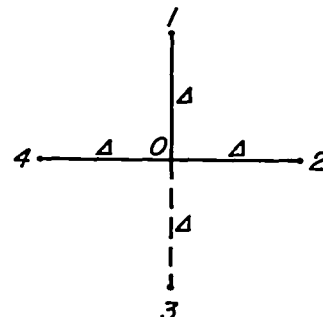
The only finite-difference equations common to the problems for ψ'_A and ψ'_B but not found in the problem for $\bar{\psi}$ derive from the boundary condition on the horizontal axis (see sketches (e) and (f)). This condition is given for both problems by equation (38) and is $\psi'_\theta(\eta, 0) = 0$ for $\eta \leq -1$. In the previous work, the finite-difference equations for lattice points located on a boundary were obtained by approximation to the boundary condition itself. In the present case, the approximation to the differential equation will be employed, and the boundary condition incorporated through use of the equivalent symmetry property.

Consider a typical point 0 on the horizontal axis as shown in sketch (g). Point 3 is a fictitious lattice point located below the horizontal axis at $\theta = -\Delta$, where Δ is the lattice interval. The finite-difference approximation to the differential equation (20) of the present text is given by equation (20) of reference 3 as

$$\psi'_2 + \psi'_4 - 2\eta_0(\psi'_1 + \psi'_3) - 2(1-2\eta_0)\psi'_0 = 0 \quad (A1)$$

where η_0 is the abscissa of point 0. The symmetry property leading to the boundary condition (38) requires that $\psi'_3 = \psi'_1$, so that for points on the horizontal axis equation (A1) reduces to

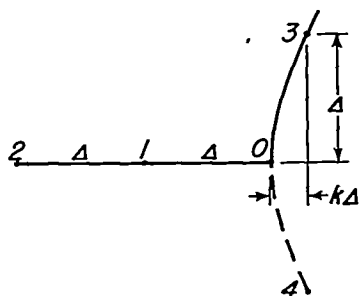
$$\psi'_2 + \psi'_4 - 4\eta_0\psi'_1 - 2(1-2\eta_0)\psi'_0 = 0 \quad (A2)$$



Sketch (g)

The point at the intersection of the horizontal axis and the shock polar needs special consideration. Sketch (h) shows conditions at this point.

Sketch (h) shows conditions at this point. Here, as before, point 4 is a fictitious point located below the boundary symmetrical to point 3. It follows from the boundary conditions (25) and (38), both of which must be satisfied at the point 0, that the first derivatives in the coordinate directions are both zero at that point. On the basis of this fact, if the function $\psi'(\eta, \theta)$ is expanded in a two-dimensional Taylor's series about point 0, the following finite-difference relations for the second derivatives are easily obtained:



Sketch (h)

$$\Delta^2 \psi'_{\eta\eta}|_0 = 4\psi'_1 - \frac{1}{2}\psi'_2 - \frac{7}{2}\psi'_0$$

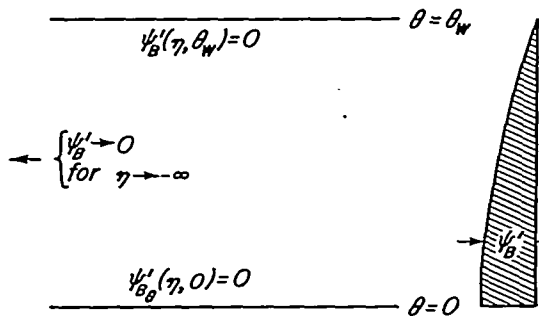
$$\Delta^2 \psi'_{\theta\theta}|_0 = 2\psi'_3 - 2\psi'_0 - k^2 \Delta^2 \psi'_{\eta\eta}|_0$$

Here the symmetry property about the horizontal axis has been used to equate ψ'_4 to ψ'_3 . Substitution of these relations into equation (20) for $\eta = -1$ leads to the following finite-difference equation for the point 0:

$$4(1-2k^2)\psi'_1 - \frac{1}{2}(1-2k^2)\psi'_2 + 4\psi'_3 - \left[4 + \frac{7}{2}(1-2k^2) \right] \psi'_0 = 0 \quad (A3)$$

Finite-Difference Equations Special to ψ'_B

The only finite-difference equation special to the problem for ψ'_B is the one used to terminate the field of computation at some vertical line on the left. As in the corresponding work for ψ , this equation is derived from an asymptotic solution of the boundary-value problem valid for large negative values of η . The derivation is parallel to that described in detail on pages 16 and 17 of reference 3.



The boundary conditions which must be satisfied by ψ'_B at large negative values of η are shown in sketch (i). The shaded section shows the anticipated variation of ψ'_B for constant η . A solution of the differential equation which satisfies the given boundary conditions is

Sketch (i)

$$\psi'_B(\eta, \theta) = \sum_{n=1}^{\infty} C_n \cos\left(\frac{n\pi\theta}{2\theta_w}\right) \times \sqrt{-\eta} K_{1/3}\left[\frac{n\pi}{6\theta_w} (-2\eta)^{3/2}\right]$$

where $K_{1/3}$ is the modified Bessel function of the second kind of order $1/3$ and the C_n are appropriate constants. If only the leading term of this solution is used and the Bessel function is replaced by the first term of its asymptotic expansion, there results

$$\psi'_B(\eta, \theta) = C \cos\left(\frac{\pi\theta}{2\theta_w}\right) \times (-\eta)^{-1/4} \exp\left[-\frac{\pi}{6\theta_w} (-2\eta)^{3/2}\right]$$

As in the earlier work, let Δ denote the lattice interval and β some large negative value of η such that $\Delta/\beta \ll 1$. It then follows from the foregoing solution that, to a first order and for a given value of θ ,

$$\frac{\psi'_B(-\beta-\Delta, \theta)}{\psi'_B(-\beta, \theta)} = \left(1 - \frac{\Delta}{4\beta}\right) \exp\left(-\frac{\pi\Delta}{2\theta_w} \sqrt{2\beta}\right) \quad (\text{A4})$$

By substituting this relation into equation (A1), a finite-difference equation can be obtained which is valid for points on the line $\eta = -\beta$ and does not include any points to the left of this line (cf. equation (22) of reference 3).

Finite-Difference Equations Special to ψ'_A

The only equations special to the problem for ψ'_A arise as a consequence of the condition along the upper boundary, where the values of ψ'_A are prescribed as a function of η . Along most of the boundary, this condition can be met by substituting the prescribed values directly into finite-difference equations of the type (A1) for points one interval below the boundary. Because of the nature of the boundary values near $\eta = 0$, however, some change from previous procedures is necessary in the vicinity of the shoulder. Modification is also required in the equations used to terminate the field on the left.

Points near shoulder of wedge. - From the known behavior of $\bar{\psi}$ in the vicinity of the shoulder (see Guderley's results, reference 13, for the flow around a convex corner), it can be shown that the variation of ψ'_A along the upper boundary near $\eta = 0$ must be of the form

$$\psi'_A(\eta, \theta_w) = \bar{\psi}_\theta(\eta, \theta_w) = D (-\eta)^{1/2} \quad (\text{A5})$$

where D is a constant of proportionality. A singular solution of the differential equation (20) which is valid in the vicinity of the shoulder

and which satisfies the boundary condition (A5) is also obtainable from Guderley's results. This solution is, in the present notation,

$$\psi'_{A_s}(\eta, \theta) = D (-\eta)^{1/2} (1-\xi)^{1/6} F\left(-\frac{1}{6}, \frac{1}{3}, \frac{1}{2}; \frac{\xi}{\xi-1}\right) \quad (A6)$$

where F is the hypergeometric function and $\xi = \xi(\eta, \theta)$ is defined by

$$\xi \equiv \frac{9}{8} \frac{(\theta_w - \theta)^2}{\eta^3}$$

Equation (A6) is suitable for use near the upper boundary ($\theta \approx \theta_w$, $\xi \approx 0$). Near the sonic line ($-\eta \approx 0$, $\xi \approx -\infty$) the following alternate form is available:

$$\begin{aligned} \psi'_{A_s}(\eta, \theta) = & \frac{D}{2^{2/3}} \left\{ \left[(-\eta)^3 + \frac{9}{8} (\theta_w - \theta)^2 \right]^{1/6} F\left(-\frac{1}{6}, \frac{1}{3}, \frac{2}{3}; \frac{1}{1-\xi}\right) + \right. \\ & \left. \frac{(-\eta)^{1/2}}{2^{2/3}(1-\xi)^{1/6}} F\left(\frac{1}{6}, \frac{2}{3}, \frac{4}{3}; \frac{1}{1-\xi}\right) \right\} \end{aligned} \quad (A7)$$

If equation (A7) is evaluated on the sonic line, there results

$$\psi'_{A_s}(0, \theta) = \frac{3^{1/3}}{2^{7/6}} D (\theta_w - \theta)^{1/3} \quad (A8)$$

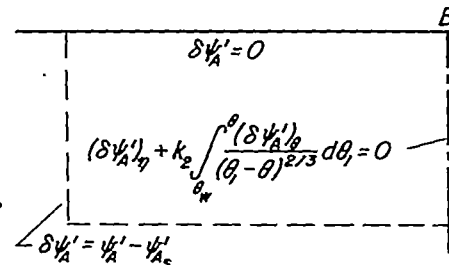
This result is in agreement with equation (32), which was developed from other considerations. It is apparent from equations (A5) and (A8) that a solution for ψ'_A will have a singularity in the first derivatives at the point $\eta = 0$, $\theta = \theta_w$.

Because of the foregoing singularity, a direct numerical calculation of ψ'_A might be expected to run into difficulty in the vicinity of the shoulder. Attempts along these lines lead, in fact, to the unlikely result of negative lift over a small region of the profile just forward of the midchord. Reductions of the lattice interval to quite small values served merely to decrease the extent of this region. This is in contrast to the previous work for ψ (and for ψ'_B as well), in which the singularity at the shoulder appears in the second derivatives. In that case, a sufficiently accurate solution for the unknown function could be obtained by direct calculation. In the present work, it was found necessary to subtract out the singularity in the first derivatives according to the following procedure:

Let a function $\delta\psi'_A$ be defined such that

$$\delta\psi'_A \equiv \psi'_A - \psi'_{A_s}$$

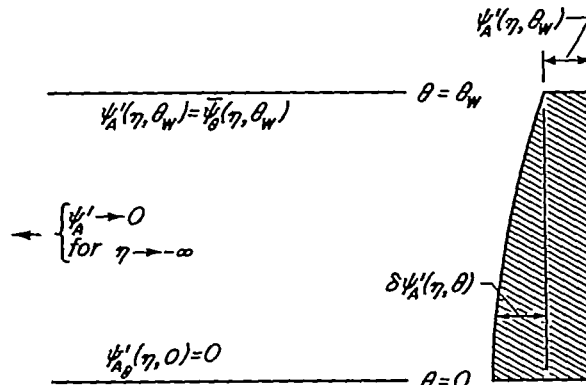
where Ψ'_{A_s} is a singular solution of the type given by equations (A6) and (A7). If the actual, numerically determined values of $\Psi'A$ on the upper boundary are examined, it is found that for a small length of the boundary near the shoulder these values can be replaced to a good approximation by a 1/2-power variation of the form given by equation (A5). This is done, and the constant D is determined such that within this length of boundary $\Psi'_{A_s}(\eta, \theta_w) = \Psi'A(\eta, \theta_w)$ or $\delta\Psi'A = 0$. On this basis, a boundary-value problem for $\delta\Psi'A$ can be defined for a small region near the shoulder as shown in sketch (j). The problem for $\delta\Psi'A$ within this region is solved jointly with the problem for $\Psi'A$ in the remainder of the field. The two regions are fitted together by the use of overlapping lattices, much as is done in the case of a graded mesh (see reference 15). The only difference is that equation (A9) must now be utilized to make the transition between the two lattices at all their common points. It is seen from sketch (j) that conditions for $\delta\Psi'A$ on both the upper boundary and sonic line are identical with the corresponding conditions for Ψ . The finite-difference equations for the calculation of $\delta\Psi'A$ can therefore be taken over directly from the previous work.



Sketch (j)

As nearly as one can judge from experience with various lattice spacings, results obtained by the foregoing process are quantitatively as well as qualitatively reliable. The primary source of error is in replacing the actual values of $\Psi'A$ along the upper boundary by a 1/2-power variation. Since the region over which this is done in the hodograph corresponds to a very small portion of the chord in the physical plane, errors from this source are probably small.

Points far to the left. - The boundary conditions for $\Psi'A$ at large negative values of η are shown in sketch (k). From the asymptotic solution for the basic problem (equation (21) of reference 3), the expression for $\Psi'A$ along the upper boundary is found to be



Sketch (k)

$$\psi'_A(\eta, \theta_w) = \bar{\psi}_\theta(\eta, \theta_w) = E(-\eta)^{-1/4} \exp \left[-\frac{\pi}{3\theta_w} (-2\eta)^{3/2} \right] \quad (A10)$$

where E is a constant.

Because of the nature of the boundary condition (A10), it is not possible to write an asymptotic solution for ψ'_A for large negative η in a single term. For this reason, the procedure previously used to terminate the field of calculation at some location on the left cannot be applied in the present case. An alternative procedure, somewhat more arbitrary in nature, can be devised by writing ψ'_A in the form

$$\psi'_A(\eta, \theta) = \psi'_A(\eta, \theta_w) + \delta\psi'_A(\eta, \theta) \quad (A11)$$

where $\delta\psi'_A$ is now defined by $\delta\psi'_A(\eta, \theta) \equiv \psi'_A(\eta, \theta) - \psi'_A(\eta, \theta_w)$ (see sketch). The attenuation of ψ'_A in going from a point at $\eta = -\beta$ to a point at $\eta = -\beta - \Delta$ is then found by treating each of the terms in equation (A11) as an independent quantity. The attenuation of $\psi'_A(\eta, \theta_w)$ is found from equation (A10) by a procedure similar to that used in obtaining equation (A4). The result is

$$\psi'_A(-\beta - \Delta, \theta_w) = \left[\left(1 - \frac{\Delta}{4\beta} \right) \exp \left(-\frac{\pi\Delta}{\theta_w} \sqrt{2\beta} \right) \right] \psi'_A(-\beta, \theta_w) \quad (A12)$$

To obtain a corresponding equation for $\delta\psi'_A$, it is assumed that for a given value of θ this quantity attenuates in the same manner as was previously found for ψ'_B . One thus has from equation (A4)

$$\delta\psi'_A(-\beta - \Delta, \theta) = \left[\left(1 - \frac{\Delta}{4\beta} \right) \exp \left(-\frac{\pi\Delta}{2\theta_w} \sqrt{2\beta} \right) \right] \delta\psi'_A(-\beta, \theta) \quad (A13)$$

Substitution of these expressions in equation (A11) for $\eta = -\beta - \Delta$ gives finally

$$\begin{aligned} \psi'_A(-\beta - \Delta, \theta) &= \left(1 - \frac{\Delta}{4\beta} \right) \exp \left(-\frac{\pi\Delta}{2\theta_w} \sqrt{2\beta} \right) \times \\ &\quad \left\{ \left[\exp \left(-\frac{\pi\Delta}{2\theta_w} \sqrt{2\beta} \right) - 1 \right] \psi'_A(-\beta, \theta_w) + \psi'_A(-\beta, \theta) \right\} \end{aligned} \quad (A14)$$

Since $\psi'_A(-\beta, \theta_w)$ is a known quantity for any given value of β , this equation can be used to terminate the field of calculation in the same manner as was done with equation (A4). The considerable element of arbitrariness in the derivation of equation (A14) can be tolerated since the over-all solution is insensitive to changes in the left-hand portion of the field.

Solution of Finite-Difference Equations

The techniques used to obtain a solution of the finite-difference equations for ψ'_A and ψ'_B were the same as those described in reference 3 for the basic solution of ψ . In general, the graded lattice as used for ψ (see fig. 2 of reference 3) was suitable for the solution of ψ'_B . For ψ'_A , however, different gradations were necessary with the smallest lattice spacing being used near the shoulder (point B of sketch (e)). The value of ψ'_B at the intersection of the shock polar and the sonic line was chosen as 10,000 so that the previously obtained values of ψ could be used to provide the initial guess for ψ'_B .

In the course of the present work, a useful technique was found for locating regions of relatively large error in the numerical solution. By use of one form of Green's theorem plus the differential equation (20), it can be shown that around any contour enclosing a region in which equation (20) is satisfied the following relation must hold:

$$\oint (2\eta \psi'_\theta d\eta + \psi'_\eta d\theta) = 0 \quad (A15)$$

In a numerical solution the line integral in equation (A15) will not, except by rare coincidence, be precisely zero around any given contour. The amount by which it differs from zero may be taken as a rough measure of the adequacy of the numerical solution over the region within the contour. If the entire field of calculation is subdivided into a number of contiguous regions, it is thus possible, by evaluating the integral around each of the enclosing contours, to locate regions within which the error is relatively high. The solution in these regions can then be improved by advancing locally to a finer mesh. This technique was found to be of great help in the present work. It would probably be useful in other elliptic boundary-value problems for which a relation analogous to equation (A15) can be obtained.

APPENDIX B
CALCULATION OF FLOW OVER REAR WEDGE
IN PHYSICAL PLANE

The procedure used to calculate the flow over the rear wedge has been outlined in the section METHOD OF SOLUTION. The fundamental operation is to determine, by stepwise methods, the initial rate of movement of the known intersection points in the basic characteristics net. The methods which are used depend on the fact that these points are, by virtue of the basic characteristics construction, points of fixed η, θ (cf. equations (55) and (57) of reference 3).

The first step is to determine the initial rate of movement of those points at which the Mach lines of the basic characteristics net meet on the sonic line. For this purpose, consider equations (48), which give the initial rate of movement of a general point of fixed η, θ . If these equations are specialized to apply to points on the sonic line, the following relations are obtained:

$$X'(0, \theta) = \frac{1}{4\bar{I}_W} \int_{\theta_W}^{\theta} \psi' \eta d\theta \quad (\text{Bl}a)$$

$$Y'(0, \theta) = \frac{(2\theta_W)^{1/3}}{4\bar{I}_W} \psi'. \quad (\text{Bl}b)$$

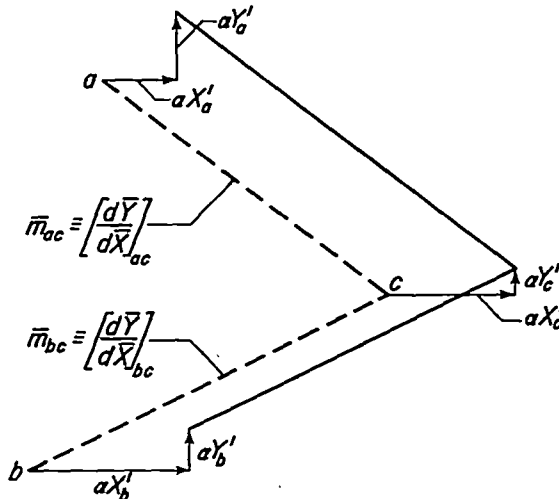
To write equation (Bl)a) the path of integration in equation (48a) is taken along the upper boundary from 0 to B (see sketch (e) on page 21) and thence downward along the sonic line. The contribution of the portion from 0 to B is zero by virtue of the condition (37). In applying these equations, the value of \bar{I}_W is known from the basic solution. The integral in equation (Bl)a) is evaluated by mechanical integration of a curve of numerically determined derivatives. Proper allowance is made for the singularity at the shoulder by integrating the singular solution analytically. The component rates of movement of the sonic point at the shoulder are both seen to be zero.

The next step in the solution is to calculate the rate of movement of intersection points downstream of the sonic line. This is done by proceeding stepwise along consecutive downgoing characteristics.

Consider three typical net points as shown in sketch (1) (cf. also fig. 4 of reference 3). The dashed lines represent the original position of the Mach lines through points a , b , and c , and the solid lines represent their displaced positions corresponding to a small, finite angle of attack α .

Since the intersection points in the Mach net are points of fixed η, θ , the components of their displacement are given by $\alpha X'$ and $\alpha Y'$. The slope of each segment of Mach line is taken, in accord with the procedures of reference 3, as the average of the slopes calculated at the two end points. The slope calculated at each end point depends, in turn, only on the value of η at that point (cf. equation (54) of reference 3).

It is desired now to determine X' and Y' at point c in terms of X' and Y' at points a and b . Since the value of η at a given net point is the same in the displaced and undisplaced positions, it follows from what has been said above that each segment of Mach line must retain its original slope after displacement. If this slope is denoted by \bar{m} , the following relations are then readily obtained:



Sketch (1)

$$X'_c = \frac{Y'_a - Y'_b + \bar{m}_{bc}X'_b - \bar{m}_{ac}X'_a}{\bar{m}_{bc} - \bar{m}_{ac}} \quad (B2a)$$

$$Y'_c = \frac{\bar{m}_{bc}Y'_a - \bar{m}_{ac}Y'_b + \bar{m}_{ac}\bar{m}_{bc}(X'_b - X'_a)}{\bar{m}_{bc} - \bar{m}_{ac}} \quad (B2b)$$

With these relations, it is a simple matter to calculate the initial rates of movement of successive net points on consecutive downgoing characteristics. For the first characteristic to be considered, point b is taken at the shoulder of the profile, where X' and Y' are both zero. Thus, X'_c and Y'_c for net points on this characteristic can be determined solely in terms of X'_a and Y'_a and the slopes \bar{m}_{ac} and \bar{m}_{bc} . For the remainder of the downgoing characteristics, X'_b and Y'_b are

known from calculations along the characteristic immediately preceding. The actual calculations can be carried out in straightforward tabular form.

The foregoing procedure enables the calculation of X' and Y' for all net points except the ones originally at the surface of the rear wedge. For these points, consideration must be given to the required boundary condition at the surface. This boundary condition is

$$\theta(X, +0; \alpha) = -(\theta_w + \alpha) \quad (B3)$$

from which it follows that

$$\theta'(X, +0) = -1 \quad (B4)$$

The problem now is to determine X' and Y' at the surface of the wedge in such a way that equation (B4) is satisfied. To do this equation (53b) is first specialized to the surface of the wedge, where it is readily shown that $\bar{x}_\theta = \bar{y}_\eta = 0$. In view of condition (B4), there results

$$Y'(\eta, -\theta_w) = \bar{Y}_\theta(\eta, -\theta_w) \quad (B5)$$

The value of Y' at points originally on the surface of the wedge is thus fixed directly by the basic solution. The corresponding value of X' can be found from a construction analogous to that of sketch (1) and is

$$X'_c = \frac{Y'_a - Y'_c - \bar{m}_{ac} X'_a}{-\bar{m}_{ac}} \quad (B6)$$

The point c is now the point originally on the surface of the wedge (i.e., Y'_c is as given by equation (B5)), and the remaining notation is the same as in sketch (1).

Application of equation (B5) requires the knowledge of $\bar{Y}_\theta(\eta, -\theta_w)$, which in the case of the wedge profile is equal to $1/\bar{\theta}_Y$. Evaluation of the latter derivative can be carried out directly from the basic Mach net, but the procedures are cumbersome and inaccurate. A better method is to use the equations of motion (cf. equation (6) of reference 4) to express $\bar{\theta}_Y$ in terms of $\bar{\eta}_X$. Following this procedure, one obtains finally

$$\bar{Y}_\theta(\eta, -\theta_w) = \frac{(2\theta_w)^{1/3}}{2\bar{\eta}(\bar{x}, 0)\bar{\eta}_X(\bar{x}, +0)} \quad (B7)$$

The quantities $\bar{\eta}$ and $\bar{\eta}_X$ which appear here are easily evaluated from the basic solution for the chordwise distribution of $\bar{\eta}$.

The preceding equations enable the calculation of the initial rate of movement X' for points originally on the surface of the rear wedge. The final step is to determine the corresponding distribution of lift. For this purpose, equation (53a) is specialized to points on the rear wedge to obtain

$$\eta'(X, +0) = - X'(\eta, -\theta_w) / \bar{X}_{\bar{\eta}}(\bar{\eta}, -\theta_w)$$

which, in view of the boundary conditions, can be shown to be equivalent to

$$\eta'(X, +0) = - X'(\eta, -\theta_w) \bar{\eta}_X(\bar{X}, +0) \quad (B8)$$

The distribution of lift is then obtained from equation (57).

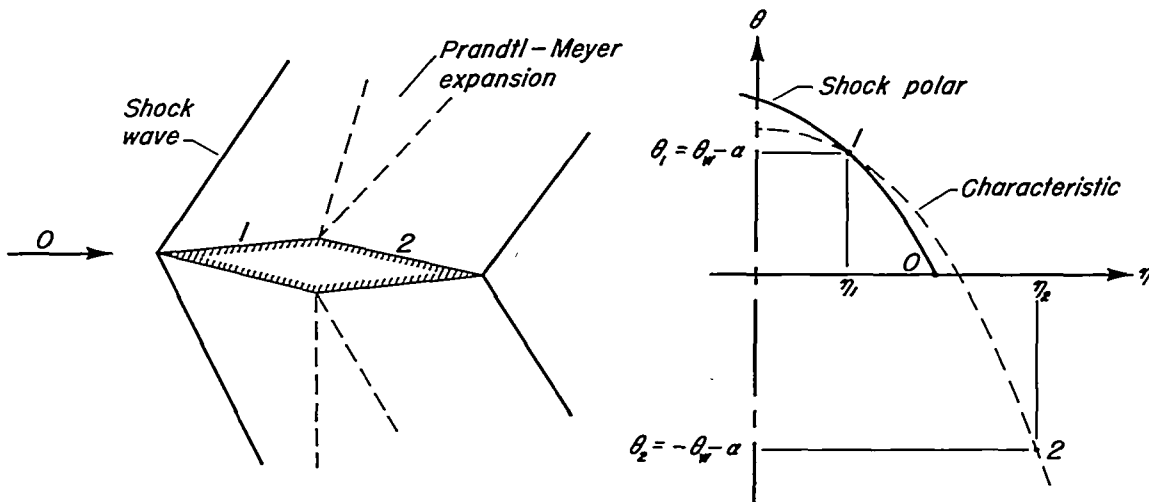
APPENDIX C

SOLUTION OF PROBLEM FOR COMPLETELY SUPERSONIC FLOW

Calculation of Lift-Curve Slope and
Center of Lift

If conditions are such that $\xi_0 \geq 2^{1/3} = 1.260$ (corresponding to $\theta_w \leq 1$; cf. equation (13)), then the basic flow over the profile at zero angle of attack is completely supersonic. The solution for the lift-curve slope and center of lift at a vanishingly small angle of attack can then be carried out analytically as follows:

Consider a completely supersonic flow about the double-wedge profile at a small angle of attack. In the physical plane the flow field has the well-known appearance shown on the left in sketch (m). The corresponding hodograph of the flow along the upper surface, in terms of the



Sketch (m)

normalized small-disturbance variables η and θ , is shown on the right. The quantities θ_w and α are, as before, the half-angle of the wedge and the angle of attack (also normalized). Except for a small range of ξ_0 just above 1.260 (see below), flow conditions must be constant along each of the segments 1 and 2 of the upper surface. In the hodograph each of these segments is thus represented by a single point located as shown. It is apparent that for a given value of θ_w , the speeds η_1 and η_2 , which are the primary unknowns in the problem, are functions solely of the angle of attack α .

To find the lift-curve slope and center of lift it is necessary first to find the derivatives $\eta'_1 = (d\eta_1/d\alpha)_{\alpha=0}$ and $\eta'_2 = (d\eta_2/d\alpha)_{\alpha=0}$. This can be done with the aid of the equations for the shock polar

$$\theta = (1-\eta) \sqrt{1+\eta} \quad (C1)$$

and for the downgoing characteristic¹⁰

$$\theta = \text{constant} - \frac{2^{3/2}}{3} \eta^{3/2} \quad (C2)$$

To find η'_1 , one must utilize the boundary condition $\theta_1 = \theta_w - \alpha$. Substitution of this condition into equation (C1) provides the following implicit equation for η_1 :

$$\theta_w - \alpha = (1-\eta_1) \sqrt{1+\eta_1} \quad (C3)$$

Differentiation of this equation gives

$$\frac{d\alpha}{d\eta_1} = \frac{1+3\eta_1}{2\sqrt{1+\eta_1}}$$

From this it follows that

$$\bar{\eta}'_1 = \frac{2\sqrt{1+\bar{\eta}_1}}{1+3\bar{\eta}_1} \quad (C4)$$

where, as in the text, the bars denote the value of η_1 at $\alpha = 0$. The value of $\bar{\eta}_1$ can be found in terms of the parameter θ_w by solving equation (C3) for η_1 with α set equal to zero. The result, obtained through standard methods for the solution of cubic equations, is

$$\bar{\eta}_1 = - \frac{\sqrt{3/2} \theta_w}{2 \cos \frac{\pi-\varphi}{3}} + 1 \quad (C5)$$

where

$$\varphi = \arccos \left(\frac{3}{4} \sqrt{\frac{3}{2}} \theta_w \right)$$

¹⁰ Compare equation (53) of reference 3.

To find η'_2 , equation (C2) for the downgoing characteristic is first specialized so as to pass through the point 1. This gives

$$\theta = (\theta_w - \alpha) + \frac{2^{3/2}}{3} (\eta_1^{3/2} - \eta^{3/2})$$

Substitution of the boundary condition $\theta_2 = -\theta_w - \alpha$ then provides the result that

$$\eta_2 = \left(\eta_1^{3/2} + \frac{3}{\sqrt{2}} \theta_w \right)^{2/3}$$

Taking the derivative with respect to α , one obtains finally at $\alpha = 0$

$$\eta'_2 = \frac{\bar{\eta}_1^{1/2}}{\left(\bar{\eta}_1^{3/2} + \frac{3}{\sqrt{2}} \theta_w \right)^{1/3}} \eta'_1 \quad (C6)$$

where η'_1 is given by equation (C4) and $\bar{\eta}_1$ by equation (C5).

Since the value of η' is constant on each segment of the profile, the lift-curve slope is easily found from equation (57) and is

$$[(\gamma+1)(t/c)]^{1/3} \left(\frac{dc_l}{d\alpha} \right)_{\alpha=0} = 2(2\theta_w)^{1/3} (\eta'_1 + \eta'_2)$$

Substitution from equation (C6) gives

$$[(\gamma+1)(t/c)]^{1/3} \left(\frac{dc_l}{d\alpha} \right)_{\alpha=0} = 2(2\theta_w)^{1/3} \eta'_1 \left[1 + \frac{\bar{\eta}_1^{1/2}}{\left(\bar{\eta}_1^{3/2} + \frac{3}{\sqrt{2}} \theta_w \right)^{1/3}} \right] \quad (C7)$$

The moment-curve slope, for moments taken about the leading edge, is found to be

$$[(\gamma+1)(t/c)]^{1/3} \left(\frac{dc_m}{d\alpha} \right)_{\alpha=0} = -\frac{1}{2} (2\theta_w)^{1/3} (\eta'_1 + 3\eta'_2)$$

or

$$[(\gamma+1)(t/c)]^{1/3} \left(\frac{dc_m}{d\alpha} \right)_{\alpha=0} = -\frac{1}{2} (2\theta_w)^{1/3} \eta'_1 \left[1 + \frac{3\bar{\eta}_1^{1/2}}{\left(\bar{\eta}_1^{3/2} + \frac{3}{\sqrt{2}} \theta_w \right)^{1/3}} \right] \quad (C8)$$

The position of the center of lift is given accordingly by

$$\left(\frac{x}{c}\right)_l = - \frac{(dc_m/d\alpha)_{\alpha=0}}{(dc_l/d\alpha)_{\alpha=0}} = \frac{1}{4} \times \frac{\frac{3\bar{\eta}_1^{1/2}}{1 + \frac{[\bar{\eta}_1^{3/2} + (3/\sqrt{2})\theta_w]^{1/3}}{\bar{\eta}_1^{1/2}}}}{1 + \frac{[\bar{\eta}_1^{3/2} + (3\sqrt{2})\theta_w]^{1/3}}{\bar{\eta}_1^{1/2}}} \quad (C9)$$

In equations (C7) and (C8), the first term inside the brackets represents the contribution of the front wedge, the second term that of the rear.

Equations (C7) and (C9) are the basis for the curves shown in figures 5 and 7 for values of $\xi_0 \geq 1.260$. The results show certain curious features when the flow over the front wedge is just sonic (i.e., $\bar{\eta}_1 = 0$, $\theta_w = 1$, $\xi_0 = 1.260$). These are as follows:

(a) The lift contributed by the rear wedge is zero (see equation (C7)).

(b) The center of lift is at the quarter-chord point (follows from statement (a) plus the condition of uniform lift on the front wedge; see also equation (C9)).

(c) The rate of change with respect to ξ_0 is infinite both for the lift-curve slope of the complete profile and for the position of the center of lift (follows from differentiation of equations (C7) and (C9)).

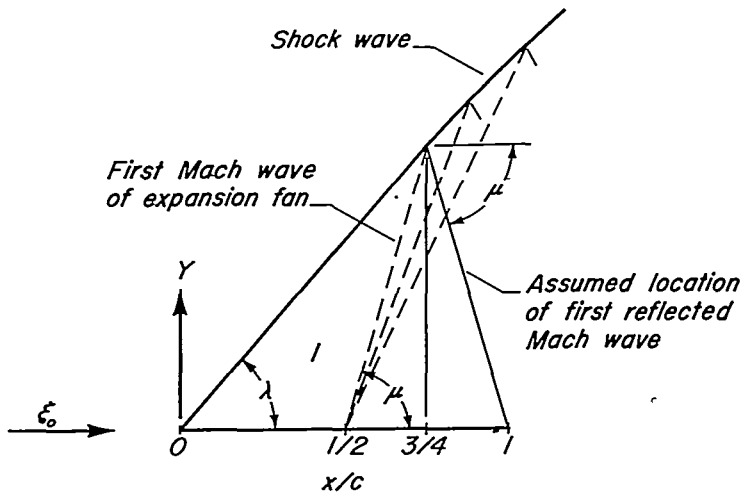
These results are associated in every case with the behavior of the lift calculated for the rear wedge.

Estimation of Lower Limit for Constant Speed Along Rear Wedge

The features just enumerated, though having a certain curiosity in themselves, cannot be accepted as completely correct. Because of interaction effects between the shock wave from the bow and the expansion fan from the shoulder, the fundamental condition of constant speed at the surface of the profile will not be satisfied along the rear wedge until the value of ξ_0 is somewhat greater than 1.260. Until then, disturbances reflected from the shock wave will reach the rear wedge and cause a slight decrease in speed toward the trailing edge. This

effect will cease when the forwardmost reflected Mach wave just touches the trailing edge. The exact value of ξ_0 at which this condition will be met is difficult to determine. An upper bound can, however, be estimated as follows:

Consider the basic flow field ($\alpha=0$) over the upper half of the profile when the first reflected Mach wave just strikes the trailing edge. Sketch (n) shows such a flow field as it would appear in transonic similarity form (cf. pp. 12-13 of reference 2). In drawing the sketch a special assumption has been introduced beyond those implicit in the small-disturbance theory; namely, that the first reflected Mach



Sketch (n)

wave is straight and has an angle of inclination μ equal to that of the first wave in the expansion fan. With this assumption, the corresponding value of ξ_0 is easily determined. Since the reflected wave must actually be curved downstream, the value so determined will be greater than the correct value for the required condition.

On the basis of sketch (n), the following equation can be written between the shock angle λ and the Mach angle μ :

$$\tan \lambda = \frac{1}{3} \tan \mu \quad (\text{C10})$$

A relation between the shock angle λ and the speed $\bar{\eta}_1$ in the region behind the shock can be obtained from equation (C3) and the known properties of the shock polar. The result is

$$\tan \lambda = \frac{(2\theta_w)^{1/3}}{\sqrt{1+\bar{\eta}_1}}$$

An analogous expression for the Mach angle μ is given by equation (54) of reference 3 and is

$$\tan \mu = \frac{(2\theta_w)^{1/3}}{\sqrt{2\bar{\eta}_1}}$$

Substitution of these relations into equation (C10) and solution for $\bar{\eta}_1$ gives

$$\bar{\eta}_1 = \frac{1}{17}$$

The accompanying value of θ_w , found from equation (C3) with $a=0$, is

$$\theta_w = 0.9685$$

This corresponds, according to equation (13), to

$$\xi_0 = 1.287 \quad (\text{C11})$$

Thus, for values of ξ_0 between 1.260 and some limit less than 1.287, the results of equations (C7), (C8), and (C9) are not exact insofar as the contribution of the rear wedge is concerned. It can be reasoned that in this range an exact solution would indicate more lift for the rear wedge than does the present analysis.

REFERENCES

1. Guderley, G., and Yoshihara, H.: The Flow Over a Wedge Profile at Mach Number 1. *Jour. Aero. Sci.*, vol. 17, no. 11, Nov. 1950, pp. 723-735.
2. Vincenti, Walter G., and Wagoner, Cleo B.: Transonic Flow Past a Wedge Profile With Detached Bow Wave - General Analytical Method and Final Calculated Results. NACA TN 2339, 1951.
3. Vincenti, Walter G., and Wagoner, Cleo B.: Transonic Flow Past a Wedge Profile With Detached Bow Wave - Details of Analysis. NACA TN 2588, 1951.
4. Cole, Julian D.: Drag of a Finite Wedge at High Subsonic Speeds. *Jour. Math. and Phys.*, vol. XXX, no. 3, July 1951, pp. 79-93.
5. Trilling, Leon: Transonic Flow Past a Wedge at Zero Angle of Attack. WADC Tech. Rep. No. 52-61, U.S. Air Force, March 1952.
6. Liepmann, H. W., and Bryson, A. E., Jr.: Transonic Flow Past Wedge Sections. *Jour. Aero. Sci.*, vol. 17, no. 12, Dec. 1950, pp. 745-755.
7. Bryson, Arthur Earl, Jr.: An Experimental Investigation of Transonic Flow Past Two-Dimensional Wedge and Circular-Arc Sections Using a Mach-Zehnder Interferometer. NACA TN 2560, 1951.
8. Griffith, Wayland: Shock-Tube Studies of Transonic Flow Over Wedge Profiles. *Jour. Aero. Sci.*, vol. 19, no 4, April 1952, pp. 249-257.
9. Guderley, Gottfried, and Yoshihara, Hideo: Two-Dimensional Unsymmetric Flow Patterns at Mach Number One. AF Tech. Rep. No. 6683, U.S. Air Force, Jan. 1952.
10. Busemann, Adolf: Application of Transonic Similarity. NACA TN 2687, 1952.
11. Spreiter, John R.: On the Application of Transonic Similarity Rules. NACA TN 2726, 1952.
12. Tricomi, F.: On Linear Partial Differential Equations of the Second Order of Mixed Type. Trans. A9-T-26, Grad. Div. of Appl. Math., Brown University, 1948.
13. Guderley, K. Gottfried: Singularities at the Sonic Velocity. Tech. Rep. F-TR-1171-ND, Air Materiel Command, U.S. Air Force, June 1948.

14. Guderley, Gottfried: Two-Dimensional Flow Patterns With a Free-Stream Mach Number Close to One. AF Tech. Rep. No. 6343, U.S. Air Force, May 1951.
15. Tasny-Tschiassny, L.: The Triangulation of a Two-Dimensional Continuum for the Purpose of the Approximate Solution of Second-Order Partial Differential Equations. Jour. App. Phys., vol. 20, no. 5, May 1949, pp. 419-424.

TABLE I.- VALUES OF ψ_B^t FOR $\theta_W = 1.6$ ($\xi_0 = 0.921$)

$-\eta$	θ	ψ_B^t									
0	1.5	199	0.1	1.1	4592	0.45	1.25	1699	1.1	0.3	316
	1.4	531		1.075	5642		1.2	2012		.2	304
	1.3	1018		1.05	7132		1.15	2332		.1	296
	1.25	1364		1.0436	7621		1.1	2629		0	294
	1.2	1826					1.0754	2755			
	1.15	2484	.125	1.125	3973				1.2	1.4	117
	1.125	2932		1.1	4764	.50	1.5	397		1.2	215
	1.1	3504		1.075	5821		1.4	817		1.0	280
	1.075	4272		1.0523	7131		1.3	1277		.8	308
	1.0625	4773					1.2	1766		.7	311
	1.05	5375	.15	1.25	1933		1.1	2207		.6	308
	1.375	6109		1.2	2563		1.0607	2324		.5	302
	1.025	7040		1.15	3470					.4	294
	1.0125	8267		1.125	4084	.6	1.5	332		.3	287
				1.1	4870		1.4	669		.2	281
.0125	1.0625	5003		1.075	5897		1.3	1008		.1	277
	1.05	5644		1.0603	6662		1.2	1326		0	275
	1.0375	6433					1.1	1568			
	1.025	7441	.175	1.125	4144		1.0119	1650	1.3	.6	258
	1.0125	8782		1.1	4902					.5	258
	1.0062	9656		1.075	5868	.7	1.5	263		.4	256
				1.0673	6221		1.4	519		.3	253
.025	1.125	3173					1.3	763		.2	251
	1.10	3805	.2	1.5	392		1.2	974		.1	249
	1.075	4666		1.4	880		1.1	1122		0	248
	1.0625	5228		1.3	1570		1.0	1173			
	1.05	5909		1.25	2047		.9311	1145	1.4	1.4	67
	1.0375	6751		1.2	2684					1.2	127
	1.025	7833		1.15	3570	.8	1.4	388		1.0	172
	1.0121	9339		1.125	4150		1.2	711		.8	201
				1.1	4862		1.1	812		.6	215
.0375	1.0625	5447		1.0733	5807		1.0	855		.4	220
	1.05	6165					.9	837		.2	221
	1.0375	7057	.225	1.125	4103					0	221
	1.025	8205		1.1	4755	.8032	.8	767	1.6	1.4	41
	1.0179	9025		1.0784	5420		.8581	.7		1.2	78
.05	1.25	1573	.25	1.25	2097			603		1.0	109
	1.2	2105		1.2	2704	.9	1.0	633		.8	133
	1.15	2875		1.15	3508		.9	636		.6	149
	1.125	3407		1.125	4008		.8	668		.4	158
	1.1	4097		1.1	4589		.7	557		0	164
	1.075	5041		1.0825	5046						
	1.0625	5657									
	1.05	6407	.275	1.125	3872	.9003	.6	497	1.8	1.4	26
	1.0375	7343		1.1	4383					1.2	50
	1.0234	8729		1.0856	4707		.9331	.5		1.0	71
								426		.8	88
.0625	1.0625	5854	.3	1.5	438					.6	101
	1.05	6630		1.4	953	.9583	.4	375		.4	110
	1.0375	7601		1.3	1635					.2	115
	1.0288	8440		1.25	2077	.9770	.3	339		0	117
.075	1.125	3625		1.15	3306	.9899	.2	317	2.0	1.4	16
	1.1	4365		1.1	4138					1.2	31
	1.075	5374		1.0877	4361	.9975	.1	304		1.0	45
	1.0625	6034								.8	57
	1.05	6830	.35	1.25	1995	1.0	1.4	212		.6	66
	1.0375	7824		1.2	2466		1.2	384		.4	73
	1.0339	8158		1.15	3012		1.0	478		.2	77
				1.1	3622		.9	490		0	78
.0875	1.0625	6194		1.0884	3766		.8	482			
	1.05	6999					.7	460			
	1.0388	7889	.4	1.5	438		.6	429			
				1.4	926		.5	396			
.1	1.5	307		1.3	1515		.4	364			
	1.4	725		1.25	1864		0	301			
	1.3	1336		1.2	2253						
	1.25	1769		1.15	2675	1.1	.8	386			
	1.2	2360		1.1	3105		.7	379			
	1.15	3223		1.0244	3231		.6	365			
	1.125	3818					.5	348			
							.4	331			



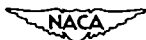
TABLE II.- VALUES OF ψ_A FOR $\theta_w = 1.6$ ($\xi_0 = 0.921$)

$-\eta$	θ	$-\psi_A$									
0	1.6	0	0.0625	1.6	2095	0.1375	1.6	3116	0.25	1.25	1877
	1.5875	1211		1.5875	2086		1.5875	2994		1.20	1664
	1.575	1489		1.575	2135		1.575	2903		1.15	1418
	1.5625	1649		1.5625	2179		1.5625	2839		1.1	1115
	1.55	1757		1.55	2210		1.55	2774		1.0825	988
	1.5375	1838		1.5375	2230		1.5375	2723			
	1.525	1894		1.525	2243		1.525	2677	.300	1.6	4206
	1.5125	1934		1.5125	2246		1.5125	2635		1.55	3629
	1.50	1967								1.5	3195
	1.475	2007	.075	1.6	2295	.15	1.6	3249		1.45	2857
	1.45	2022		1.5875	2257		1.575	3016		1.4	2581
	1.425	2014		1.575	2269		1.55	2863		1.35	2343
	1.4	1993		1.5625	2290		1.525	2748		1.3	2129
	1.35	1930		1.55	2304		1.50	2649		1.25	1925
	1.3	1844		1.5375	2312		1.475	2599		1.2	1739
	1.25	1737		1.525	2315		1.45	2472		1.15	1497
	1.20	1603		1.5125	2310		1.425	2386		1.1	1251
	1.15	1431		1.5	2303		1.4	2304		1.0877	1186
	1.10	1184		1.475	2279		1.35	2141			
	1.05	790		1.45	2244		1.3	1977	.35	1.6	4294
				1.425	2199		1.25	1802		1.55	3721
.0125	1.6	937					1.2	1602		1.5	3278
	1.5875	1380	.0875	1.6	2478		1.15	1348		1.45	2926
	1.575	1614		1.5875	2419		1.1	997		1.4	2637
	1.5625	1753		1.575	2403		1.0063	582		1.35	2391
	1.55	1846		1.5625	2401					1.3	2174
	1.5375	1914		1.55	2399	.175	1.6	3486		1.25	1974
	1.525	1962		1.5375	2394		1.575	3224		1.2	1782
	1.5125	1995		1.525	2387		1.55	3034		1.15	1593
				1.5125	2375		1.525	2886		1.1	1405
.025	1.6	1325					1.50	2761		1.0884	1362
	1.5875	1553	.1	1.6	2650		1.475	2650			
	1.575	1740		1.5875	2573		1.45	2547	.4	1.6	4259
	1.5625	1897		1.575	2534		1.425	2449		1.55	3724
	1.55	1935		1.5625	2512					1.5	3297
	1.5375	1991		1.55	2494	.2	1.6	3690		1.45	2950
	1.525	2030		1.5375	2477		1.575	3408		1.4	2662
	1.5125	2057		1.525	2460		1.55	3190		1.35	2419
	1.50	2078		1.5125	2440		1.525	3013		1.3	2207
	1.475	2097		1.50	2418		1.50	2867		1.25	2017
	1.45	2096		1.475	2372		1.475	2737		1.2	1845
	1.425	2075		1.45	2319		1.45	2620		1.15	1688
				1.425	2261		1.425	2510		1.1	1553
.0375	1.6	1623		1.40	2198		1.4	2407		1.0844	1578
	1.5875	1731		1.35	2069		1.35	2213			
	1.575	1869		1.3	1930		1.3	2027	.45	1.6	4114
	1.5625	1962		1.25	1775		1.25	1836		1.55	3643
	1.55	2025		1.20	1594		1.2	1624		1.5	3252
	1.5375	2069		1.15	1360		1.15	1366		1.45	2926
	1.525	2100		1.1	1026		1.1	1025		1.4	2653
	1.5125	2119		1.05	386		1.0733	786		1.35	2421
.05	1.6	1874	.1125	1.6	2816	.225	1.6	3862		1.3	2221
	1.5875	1911		1.5875	2721		1.575	3568		1.25	2046
	1.575	2000		1.575	2661		1.55	3329		1.2	1896
	1.5625	2069		1.5625	2621		1.525	3132		1.15	1767
	1.55	2117		1.55	2589		1.50	2964		1.1	1669
	1.5375	2149		1.5375	2560		1.475	2819		1.0754	1637
	1.525	2171		1.525	2533		1.45	2688	.5	1.6	3886
	1.5125	2182		1.5125	2505		1.425	2568		1.55	3489
	1.50	2190								1.5	3148
	1.475	2188	.125	1.6	2972	.23	1.6	4004		1.45	2856
	1.45	2169		1.5875	2862		1.575	3702		1.4	2607
	1.425	2137		1.575	2784		1.55	3149		1.35	2394
	1.4	2094		1.5625	2728		1.525	3236		1.3	2211
	1.35	1999		1.55	2682		1.5	3053		1.2	1922
	1.3	1886		1.5375	2642		1.475	2894		1.1	1743
	1.25	1755		1.525	2605		1.45	2751		1.0607	1717
	1.20	1596		1.5125	2570		1.425	2622			
	1.15	1391		1.50	2534		1.4	2502	.55	1.6	3603
	1.10	1096		1.475	2465		1.35	2282		1.55	3280
	1.05	619		1.450	2396		1.3	2079		1.5	2994
				1.425	2324						

NACA

TABLE II.-- CONCLUDED

$-\eta$	θ	$-\Psi_A$	$-\eta$	θ	$-\Psi_A$	$-\eta$	θ	$-\Psi_A$
.55	1.45	2742	1.1	1.6	727	1.6	0	389
	1.4	2525		1.5	809			
	1.35	2337		1.4	860		1.6	50
	1.3	2174		1.3	887		1.4	115
.6				1.2	897		1.2	168
	1.6	3283		1.1	894		1.0	209
	1.5	2801		1.0	881		.8	239
	1.4	2412		.9	861		.6	260
	1.3	2110		.8	835		.4	273
	1.2	1889		.7	805		.2	280
	1.1	1751		.6	771		0	283
	1.0119	1710		.5	736			
.7				.4	704	2.0	1.6	39
	1.6	2588		.3	676		1.4	69
	1.5	2345		.2	654		1.2	103
	1.4	2112		.1	641		1.0	132
	1.3	1912		0	637		.8	155
	1.2	1754					.6	172
	1.1	1643		1.2	510		.4	184
	1.0	1576		1.5	593		.2	191
	.9311	1544		1.4	653		0	193
				1.3	693			
.8	1.6	1950		1.2	718			
	1.5	1873		1.1	730			
	1.4	1766		1.0	733			
	1.3	1655		.9	728			
	1.2	1555		.8	717			
	1.1	1473		.7	701			
	1.0	1406		.6	682			
	.9	1345		.5	663			
				.4	644			
	.8032	.8	1266		.3	628		
.9	.8581	.7	1086		.2	615		
			0		.1	607		
	1.6	1438				604		
	1.5	1449	1.3	1.6	358			
	1.4	1424		1.5	434			
	1.3	1380		1.4	494			
	1.2	1329		1.3	539			
	1.1	1276		1.2	571			
	1.0	1224		1.1	592			
	.9	1169		1.0	604			
	.8	1107		.9	610			
	.7	1033		.8	610			
				.7	605			
1.0	.9003	.6	951		.6	597		
	.9331	.5	848		.5	588		
	.9583	.4	771		.4	579		
	.9770	.3	717		.3	571		
			0		.2	564		
					.1	560		
						559		
1.0	.9899	.2	677	1.4	1.6	250		
	.9975	.1	658		1.4	372		
					1.2	450		
					1.0	494		
					.8	514		
					.6	517		
					.4	512		
					.2	506		
					0	504		
1.0	1.1	1079						
	1.0	1047	1.6	1.6	120			
	.9	1009		1.4	209			
	.8	965		1.2	277			
	.7	914		1.0	325			
	.6	860		.8	356			
	.5	805		.6	374			
	.4	754		.4	384			
	0	650		.2	388			



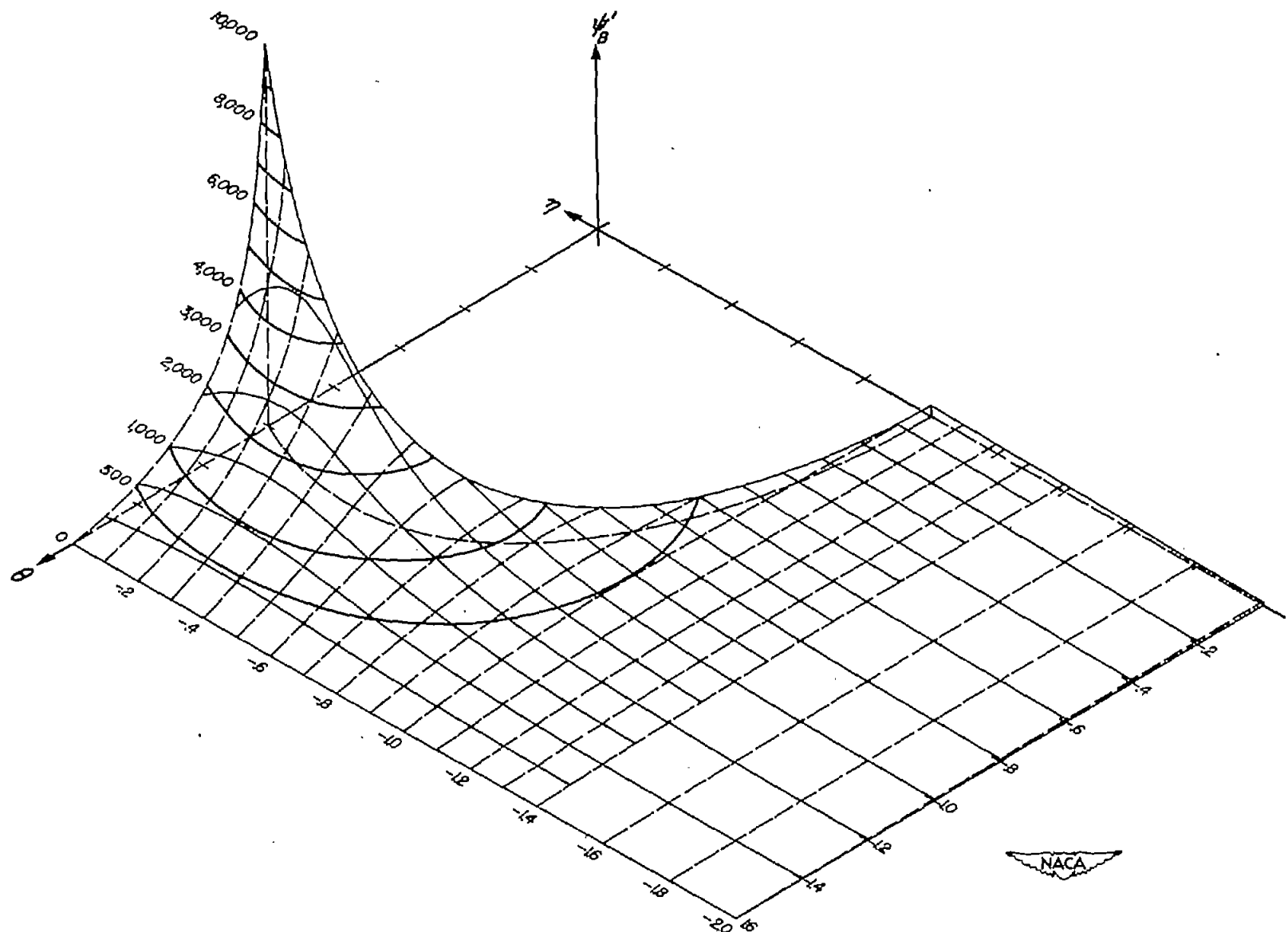


Figure 1.—The variation of ψ' as a function of η and θ for $\theta_w = 46$ ($\xi = 0.921$).

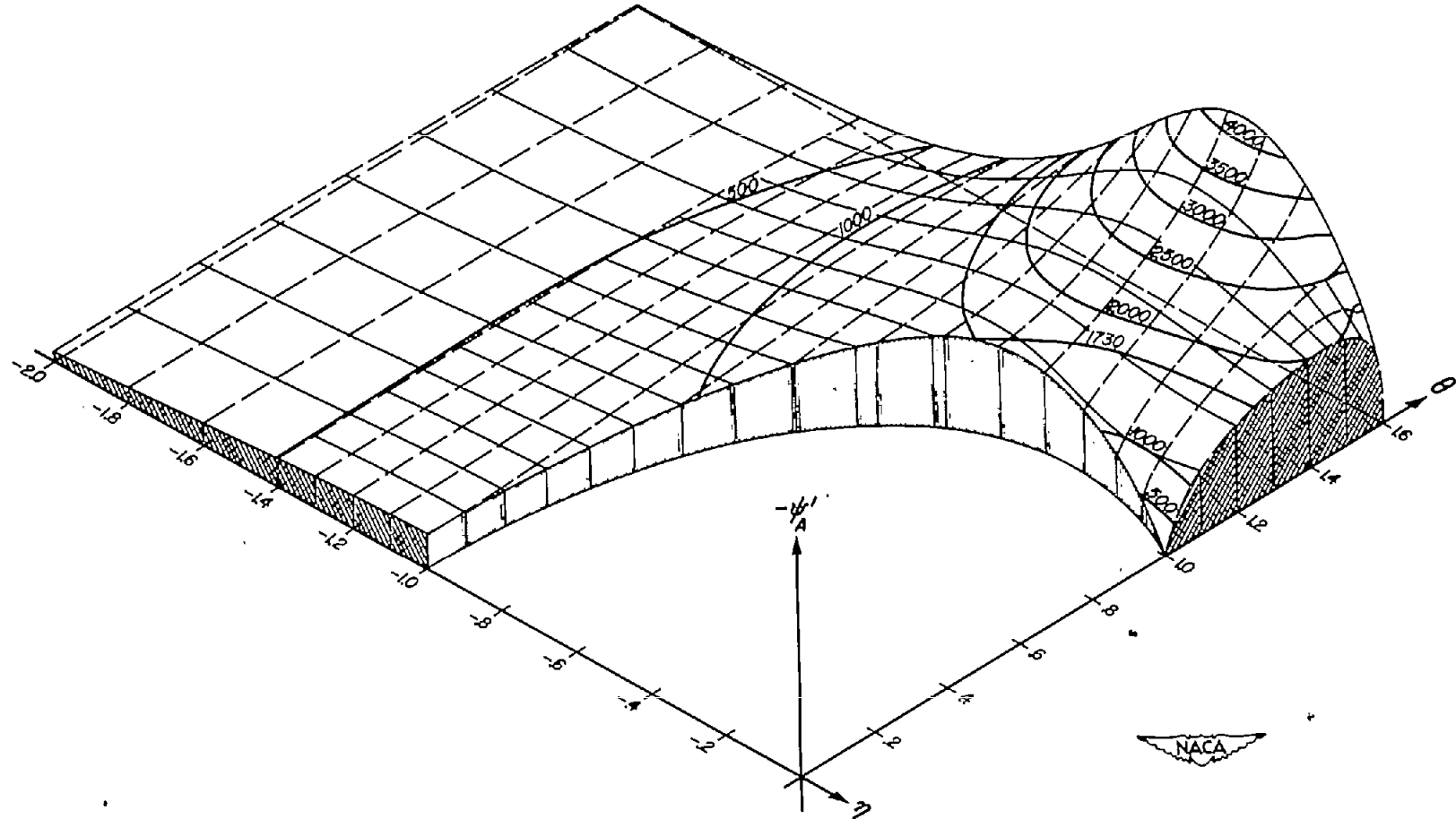


Figure 2.— The variation of ψ' as a function of η and θ for $\theta_w = 1.6$ ($\xi_0 = 0.921$).

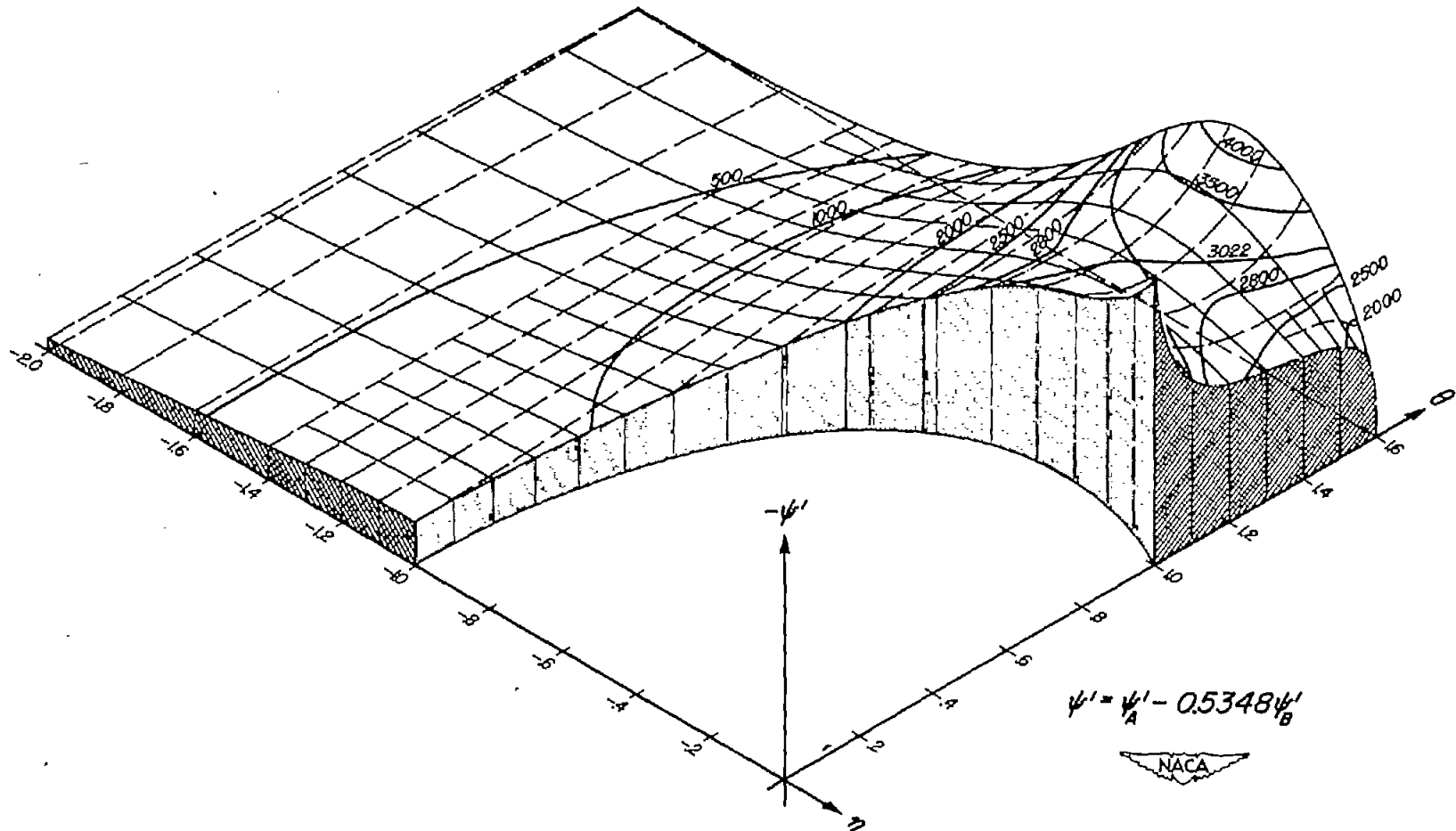


Figure 3.—The variation of ψ' as a function of η and θ for $\theta_w = 1.6$ ($\xi_0 = 0.921$).

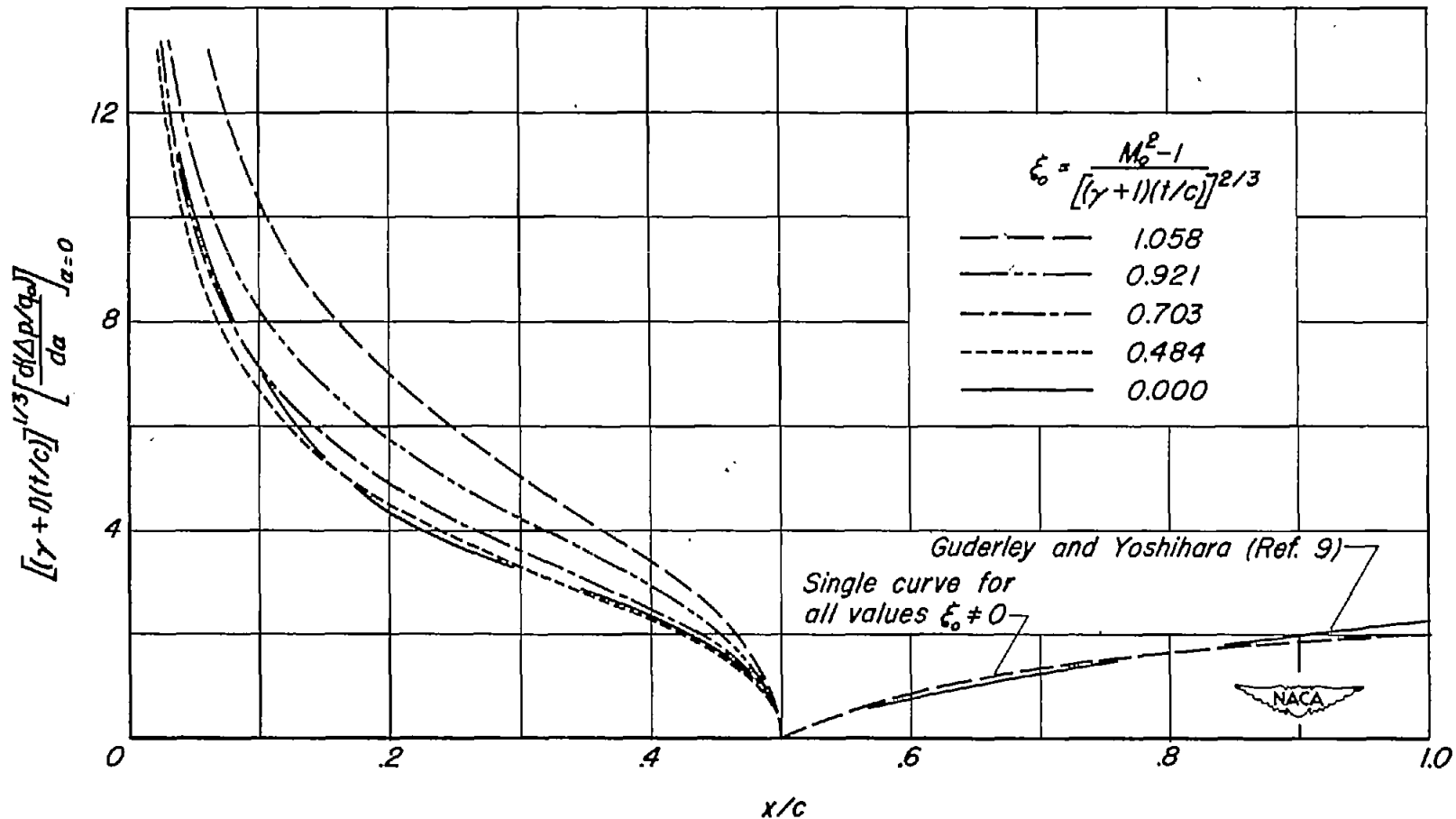


Figure 4.-Chordwise distribution of lift.

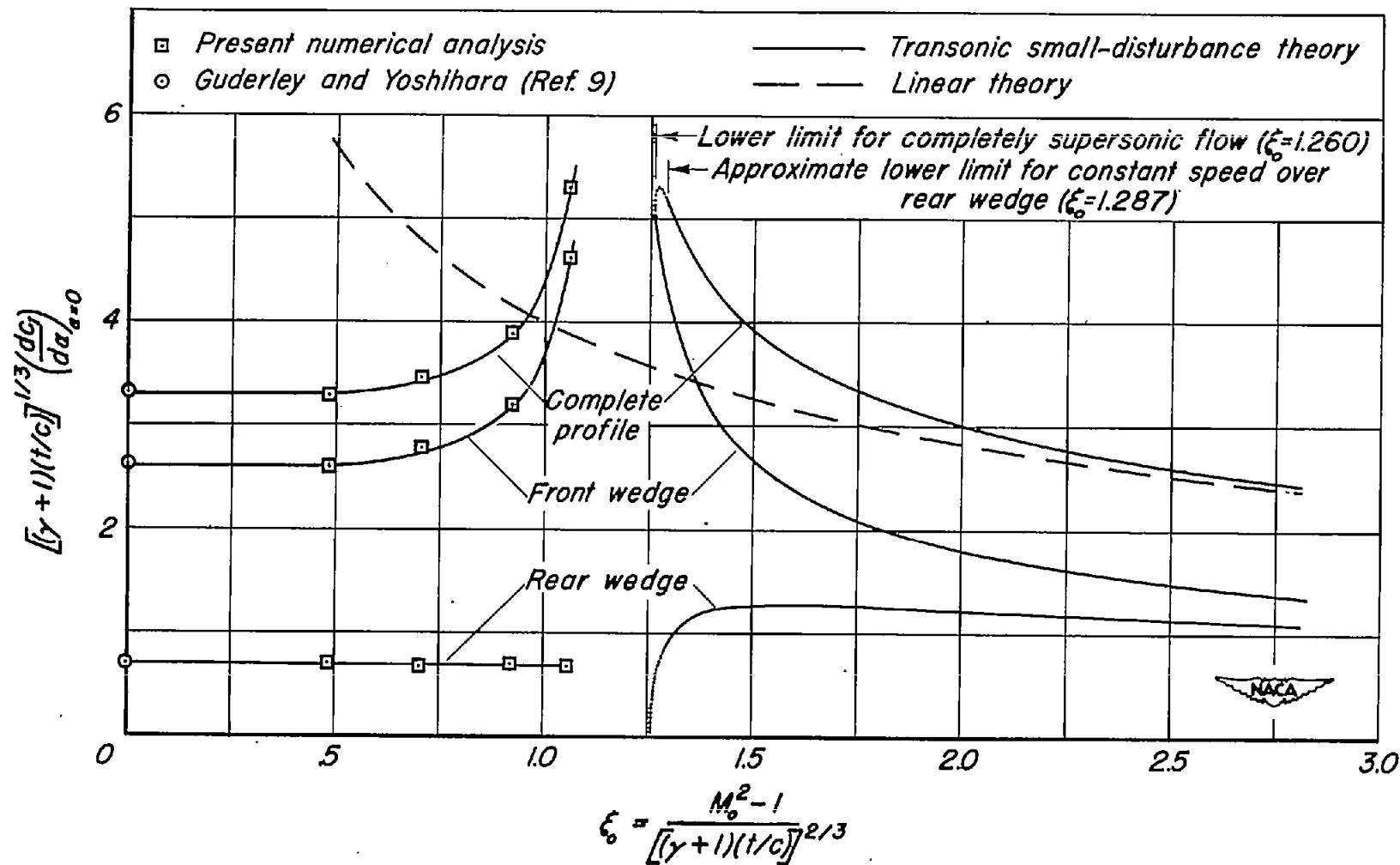


Figure 5.—Generalized lift-curve slope as a function of transonic similarity parameter.

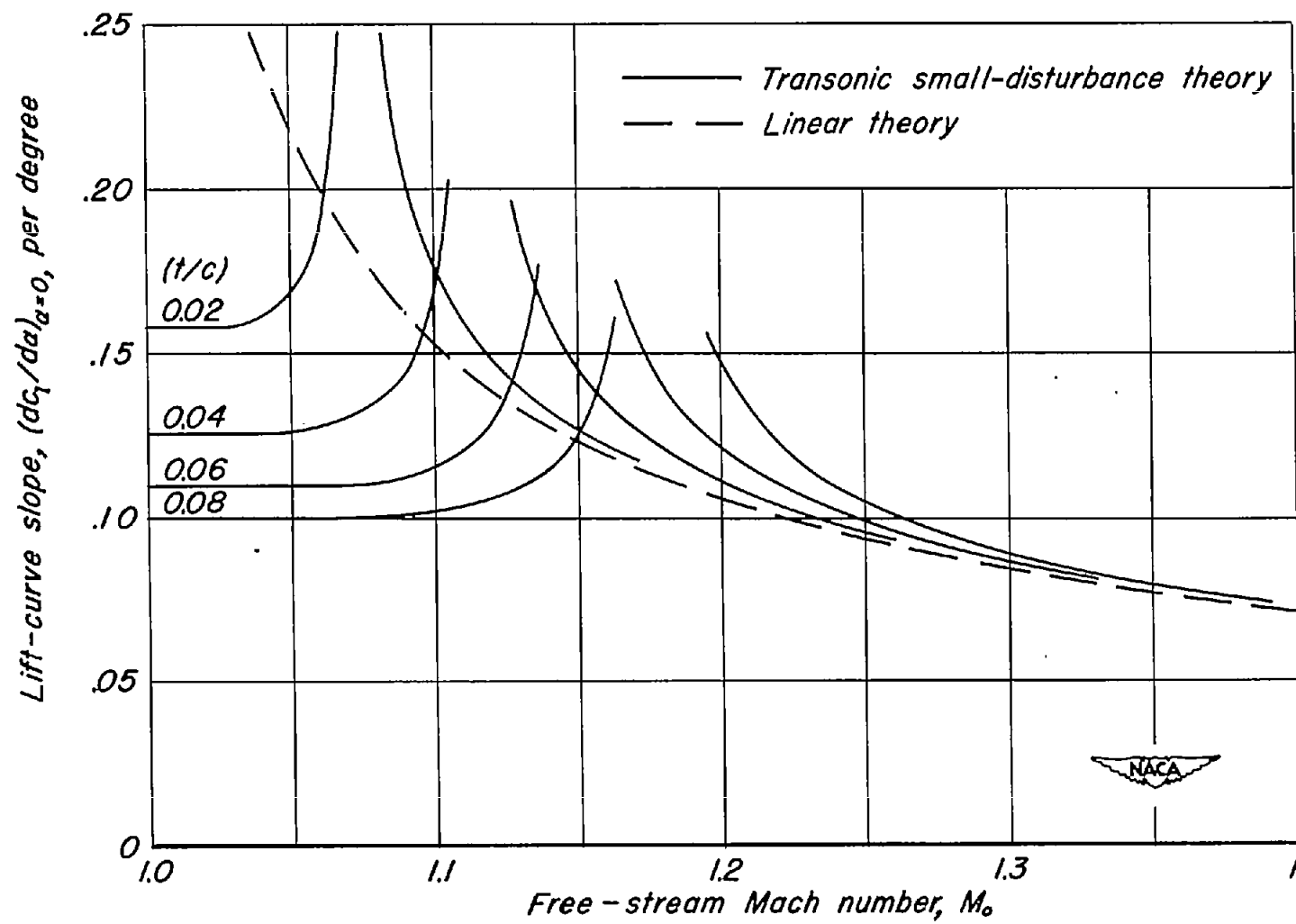


Figure 6.- Lift-curve slope as a function of Mach number for several thickness ratios ($\gamma = 1.4$).

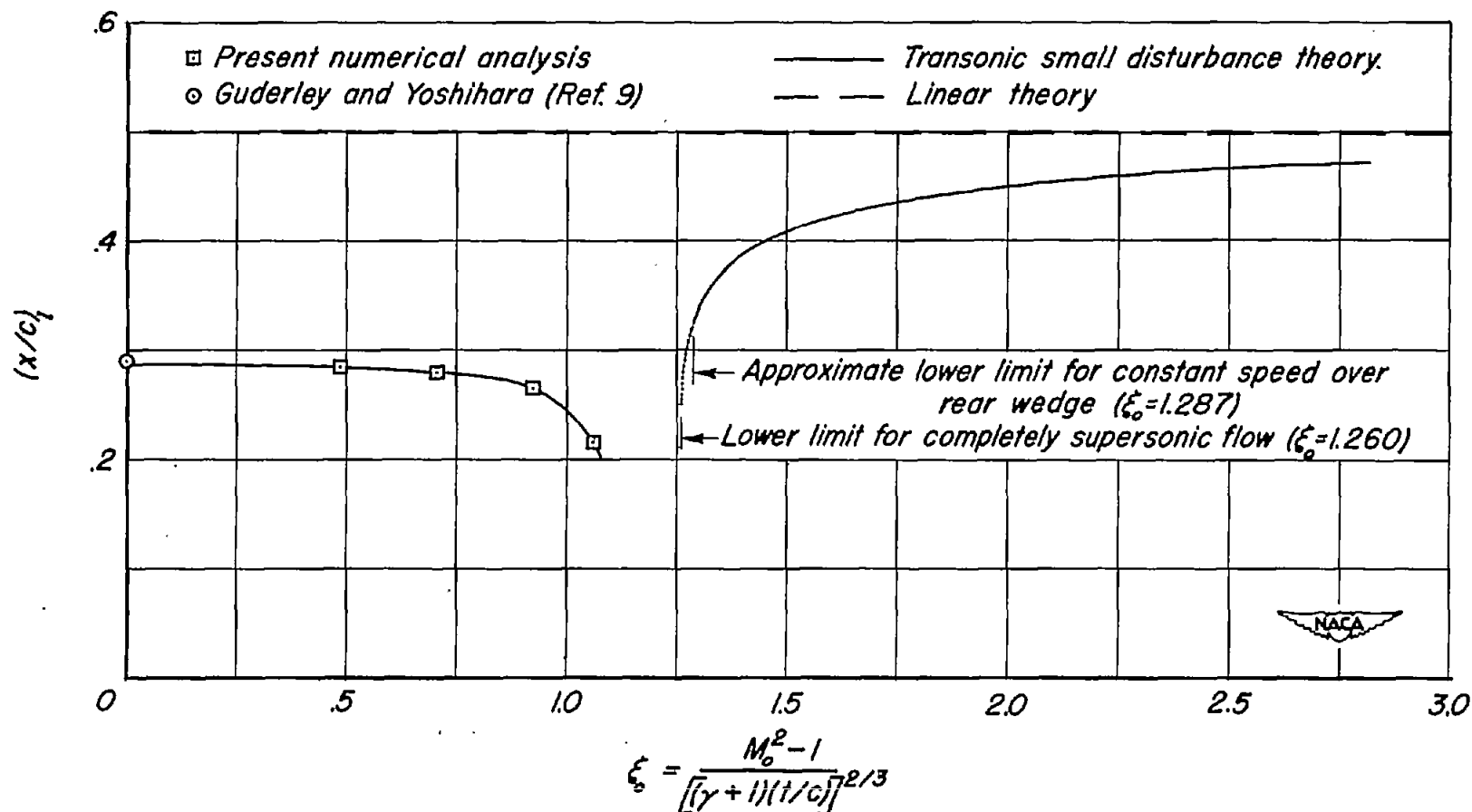


Figure 7 - Center of lift as a function of transonic similarity parameter.